A Multiphase Microscopic Diffusion Model for Stratum Corneum Permeability. I. Formulation, Solution, and Illustrative Results for Representative Compounds

TSUO-FENG WANG,[1] GERALD B. KASTING,[2] JOHANNES M. NITSCHE[1]

[1]Department of Chemical and Biological Engineering, University at Buffalo, State University of New York, Buffalo, New York 14260-4200

[2]College of Pharmacy, University of Cincinnati Medical Center, Cincinnati, Ohio 45267-0004

Received 17 December 2004; revised 20 June 2005; accepted 5 September 2005

Published online in Wiley InterScience (www.interscience.wiley.com). DOI 10.1002/jps.20509

ABSTRACT: A two-dimensional microscopic transport model of the stratum corneum (SC) incorporating corneocytes of varying hydration and permeability embedded in an anisotropic lipid matrix is presented. Results are expressed in terms of a dimensionless permeability $(\hat{P}_{SC/w})^{comp}$, which is a function of two dimensionless parameters, R and σ. R is a ratio of transbilayer to lateral molecular flows within a lipid bilayer and σ is the ratio of (lateral) permeability in the lipid phase, $D_{lip}K_{lip/w}$, to that in the corneocyte phase, $D_{cor}K_{cor/w.}$ The shape of the dimensionless permeability surface is also governed by the arrangement of the SC lipids, where Model 1 represents the extreme in which lipid-phase transport can occur with no transbilayer transport, whereas Model 2 entails maximum transbilayer transport. Model calculations are exemplified by characterizing the skin permeability of four representative permeants: water, ethanol, nicotinamide, and testosterone. A comparison with experimental steady state permeability and partition data supports that the transport properties of the SC lipids are highly anisotropic, with lateral diffusivities several orders of magnitude higher than the equivalent diffusivity calculated from transbilayer hopping. Nevertheless, the calculations suggest that corneocyte-phase transport plays a major role for all four permeants. These results confirm our previous calculations on water permeability and present a marked contrast to the commonly stated doctrine that the SC transport pathway is primarily intercellular.
 J Pharm Sci 95:620–648, 2006
Keywords: stratum corneum (SC); permeability; diffusion coefficient; partition coefficient; microstructure; intercellular lipid; corneocyte

INTRODUCTION

Quantitative aspects of the permeation of molecules through skin[1–4] (in particular, rates of permeation and differential permeability of different molecules) are central to the function of topically applied and transdermally delivered drugs,[3,5–7] as well as risk assessment of chemical exposure.[8,9] The complexity of the transdermal transport process arises from the multiphase, multiscale intricacy of skin microstructure,[2,10,11] and from the interplay of a number of microscopic physicochemical factors including partitioning and diffusion. Evidence for this complexity lies in the fact that closely related compounds (e.g., benzoic acid and hippuric acid, or nicotinic acid and nicotinamide) can exhibit vastly different rates of percutaneous penetration.[12]

This article includes Supplementary material, available at http://www.interscience.wiley.com/jpages/0022-3549/suppmat.

Tsuo-Feng Wang's present address is National Science Council, Planning & Evaluation Division, No. 106, HoPing E. Road, Sec. 2, Taipei 106, Taiwan (R.O.C.).

Correspondence to: Johannes M. Nitsche (Telephone: 716-645-2911, ext. 2213; Fax: 716-645-3822; E-mail: nitsche@eng.buffalo.edu)

Journal of Pharmaceutical Sciences, Vol. 95, 620–648 (2006)

Most important as a barrier to, and regulator of, molecular passage is the stratum corneum (SC), comprising 6–20 layers[13] of flattened, interleaved, partially desiccated, keratinized cells (corneocytes) comprising the outermost layer of the epidermis. This layer has the structure of a composite medium, the corneocytes representing obstacles embedded in a lipid matrix, which has an ordered (non-liquid-like) molecular structure.[14,15] The interiors of the corneocytes themselves have a composite ultrastructure inside the cellular envelopes, comprising keratin filaments surrounded by a lipid-protein matrix[2,16] and water of hydration. The SC serves as a barrier for access to the viable epidermis and the dermis, and thence to the dermal and ultimately systemic circulation.

Given this pivotal barrier function, the question that has been addressed most heavily in the literature on percutaneous transport is: what is the permeability coefficient $P_{SC/w}$ characterizing steady flux through the SC as a function of the chemical structure of the permeating drug or chemical solute? In the context of an *in vitro* experiment where two aqueous solution compartments are separated by an SC sample, this coefficient appears in the expression

$$J = P_{SC/w}(C_{w/1} - C_{w/2}) \qquad (1)$$

for the steady flux J of solute between the compartments, respectively at concentrations $C_{w/1}$ and $C_{w/2}$.

One fruitful avenue of investigation[17–22] has used critical analysis of a large permeability database[23,24] to produce empirical correlations for $P_{SC/w}$, usually giving $P_{SC/w}$ as a function of two types of physical parameters. The first is a thermodynamic parameter indicative of molecular affinity for the SC; owing to the importance of lipid tissue constituents, this parameter is usually taken to be the partition coefficient $K_{o/w}$ for solute distribution between octanol and water.[17,22] The second is the solute's molecular weight or volume, which is the most critical determinant of in-tissue mobility.

Although the stratum corneum is often characterized as a predominantly lipoidal barrier,[17,24–32] a growing body of evidence suggests the existence of a polar pathway representing a significant if not dominant route for permeation of many polar compounds. For instance, Peck et al.[33] found that the permeability coefficients of urea, mannitol, sucrose, and raffinose could not be explained on the basis of the well established lipid-based correlation of Potts and Guy,[17] but were consistent with a hypothetical porous polar pathway, to which they could even assign an effective pore radius (15–25 Å) on the basis of hindered diffusion theory. Ackermann and Flynn[34] concluded from studies on nude mouse skin that percutaneous absorption of urea, thiourea, glycerol, and glucose seemed to take place "mainly through hydrophilic and water-filled regions in the skin," which therefore "does not act as a simple lipoidal barrier." Anderson and Raykar[35] concluded that "lipophilicity alone, regardless of the lipophilicity scale employed, cannot account for the relative permeabilities of structurally diverse sets of compounds." This and other evidence[36–41] has prompted the inclusion of a parallel aqueous polar pathway, whose precise nature is still elusive, in a number of permeability models,[19,22,38,39,41,42] according to the reasonable engineering approximation of additive permeability for parallel pathways:

$$P_{SC/w} = (P_{SC/w})^{comp} + (P_{SC/w})^{polar}. \qquad (2)$$

The first term represents the intrinsic permeability of the composite medium represented by defect-free, appendage-free SC. Because of the emphasis on the lipid pathway noted above, this term is often regarded as synonymous, in origin and/or notation, with the permeability $(P_{SC/w})^{lip}$ of the lipid pathway. A more general view would allow for solute occupancy of the entire microstructure, which has been well documented in partitioning studies.[35,37,43] The relative contributions from lipid and corneocyte phases can then be revealed naturally by a rigorous microscopic analysis of diffusion. The second term represents contributions from any defects, skin appendages (especially hair follicles), and a possible desmosome-corneocyte pathway about which little is known.

The specific purpose of this study is to present a more detailed analysis of the intrinsic permeability $(P_{SC/w})^{comp}$ of defect-free, appendage-free SC, considered as a macroscopically observable effective property of the composite microstructure. Aside from its general importance, understanding of $(P_{SC/w})^{comp}$ is key to subtracting off the baseline contribution from basic SC microstructure in assessing appendageal and defect-related contributions to an observed overall permeability (cf. Eq. 2).

Understanding of $(P_{SC/w})^{comp}$ has seen considerable progress within the framework of so-called "brick-and-mortar" models,[24,31,32,44–51] the bricks

Table 1. Survey of Existing Brick-and-Mortar Models

Analysis	Corneocyte Shape	Lipid-Phase Diffusion	Treatment of Diffusion	Corneocyte Permeability
Yotsuyanagi and Higuchi (1972)[51]	Idealized (lamellar)	Only diff. in direction ⊥ to cell wall considered	Exact result for resistances in series	**Permeable**
Michaels et al. (1975)[44]	Idealized (rectangular)	Isotropic	Analytical approx.	**Permeable**
Albery and Hadgraft (1979)[45]	Idealized (lamellar)	**Anisotropic**	Analytical approx.	**Permeable**
Tojo (1987)[46]	Idealized (rectangular)	Isotropic	Analytical approx.	**Permeable**
Edwards and Langer (1994)[47]	Idealized (rectangular)	**Anisotropic**	Analytical approx.	**Permeable**
Heisig et al. (1996)[48]	Idealized (rectangular)	Isotropic	**Detailed numerics**	**Permeable**
Johnson et al. (1997)[24]	Idealized (rectangular)	**Anisotropic**	Analytical approx.	Impermeable
Charalambopoulou et al. (2000)[49]	Idealized (rectangular)	Isotropic	**Detailed numerics**	**Permeable**
Frasch (2002)[50]	**Realistic (from images)**	Isotropic	**Detailed numerics**	**Permeable**
Frasch and Barbero (2003)[32]	Idealized (rectangular)	Isotropic	**Detailed numerics**	Impermeable
Present analysis	**Realistic (trapezoidal)**	**Anisotropic**	**Detailed numerics**	**Permeable**

Realistic attributes are emphasized in bold.

and mortar respectively corresponding to the corneocytes and the surrounding intercellular lipid bilayers. Attributes of these models are summarized in Table 1. They have led to a basic theoretical understanding of the role of microscopic tortuosity arising from zig-zagging of the lipid pathway around the corneocyte obstacles, which has also been characterized experimentally.[29,31,52,53] The potential role of corneocyte permeability has also been well recognized.[44–51] The state of the art is represented by the particularly comprehensive models of Frasch and Barbero,[32,50] which are based upon a structural characterization of mouse skin, with detailed numerical treatment of the diffusion process[32,50] (avoiding analytical approximations for tortuosity factors[24,44,46,47]) and allowance for corneocyte permeability.[50] It is significant that no analysis to date has combined all the elements of: (i) a realistic treatment of the pointed (nonrectangular) end-shape of corneocytes, (ii) corneocyte permeability, and (iii) inherent anisotropy of lipid-phase diffusion. Our analysis offers a rigorous treatment of all three elements.[54] Moreover, it addresses head-on a significant issue, heretofore not considered, relating to the topology of the lipid phase as a lamellar medium surrounding the corneocytes. The final model yields quantitative predictions of $(P_{SC/w})^{comp}$ as a function of microscopic physicochemical properties of the permeant, for both partially hydrated and fully hydrated states of the SC, tuned with reference to human SC permeability data.

The presentation is broken down into two parts. This study gives a comprehensive account of the underlying microscopic diffusion theory, and the numerical and asymptotic methods applied to solve the multiphase transport problem formulated. In addition to discussing illustrative outcomes of the model for several representative compounds, demonstrating its practical application, we draw useful general conclusions about the microscopic mechanics of permeation. A companion study[55] develops realistic general procedures for estimating the parameters entering the model (partition and transport coefficients of both lipid and corneocyte phases, based on experimental data and theoretical considerations of geometrical exclusion and hindered diffusion in media with ultrastructure), and applies the model to a large SC permeability database.

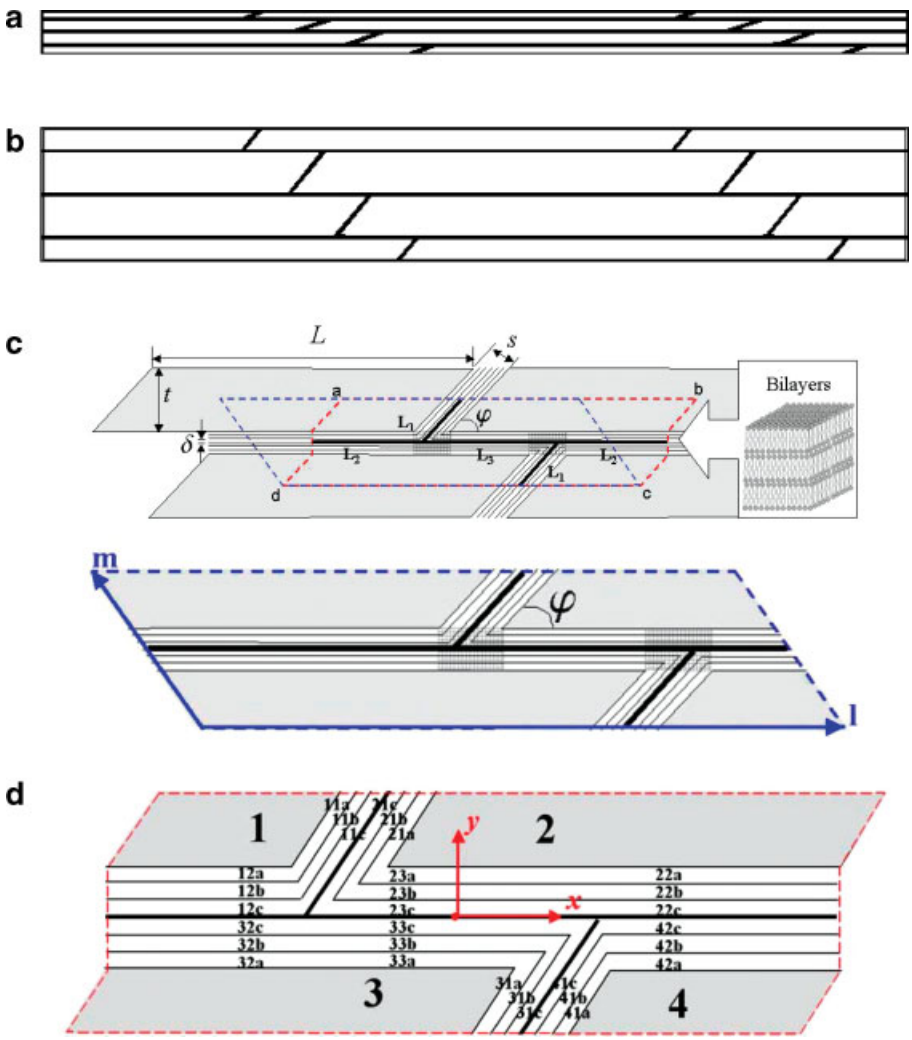

Figure 1. Definition sketch showing assumed model microstructure. (a) Structure for partially hydrated skin. (b) Structure for fully hydrated skin. (c) Schematic drawings indicating notation (not to scale). (d) Labeling scheme used to identify individual lipid bilayers and corneocytes within a unit cell.

FORMULATION OF THE MODEL

Figure 1 gives a cross-sectional view of the assumed two-dimensional structure, showing a spatially periodic "brick-and-mortar" arrangement of corneocytes embedded in a lipid matrix. Our goal is to ascertain the effective properties of this material, considered as a composite medium extending indefinitely in the x and y directions, via application of rigorous theory for diffusion in periodic composite media.[56–58] In real skin the SC constitutes a finite subset of this infinite medium extending in the y direction a distance corresponding to a number $N_{\text{layer}} = 6–20$ of cell layers.[13] For definiteness, we take $N_{\text{layer}} = 15$ as a reasonable representative value.[24]

Two states of the lipid and corneocyte phases are considered. The term "partially hydrated" refers to healthy, partially hydrated skin *in vivo*. "Fully hydrated" refers to SC that is completely swollen with water. The latter case applies to certain *in vitro* diffusion cell experiments, in which the SC membrane separating two aqueous compartments is fully saturated with water. Considerable data exist on water content of stratum corneum.[59–61] For fully hydrated SC, there is no water activity gradient across the SC because the epidermal surface is in contact with physiological saline, or the equivalent. The dermal surface is always in contact with interstitial fluids, which are osmotically equivalent to physiological saline. In partially hydrated SC, there is a water

activity gradient across the tissue, so water content (and SC permeability) changes with depth. A typical water concentration gradient in SC could run from 10 wt% at the epidermal surface to 60 wt% at the dermal surface, with an average value of 30 wt% across the tissue.[59,60] In both cases, the lower three to four layers of the SC do not appear to hydrate very much relative to the upper layers.[59,62,63] For simplicity, in either state we make the approximation of treating the SC as a vertically homogeneous tissue characterized by an average value of water content assigned below. For the fully hydrated case the simplification is that the SC is assumed to swell uniformly. For the partially hydrated case the simplification is that the water activity gradient across the SC *in vivo* has been neglected. Property variations with depth can sometimes influence drug fluxes and concentration profiles across the SC.[64,65] Nevertheless, as evidenced by the ample precedent of past brick-and-mortar models,[24,26,31,32,44–49,51] meaningful conclusions can be drawn from macroscopically homogeneous models representing an average state of the SC.

Our analysis is structured around a decomposition of the form[1,2,4,7,19,66,67]

$$(P_{\mathrm{SC/w}})^{\mathrm{comp}} = K_{\mathrm{SC/w}} D_{\mathrm{SC}} / h_{\mathrm{SC}}, \qquad (3)$$

in which $K_{\mathrm{SC/w}}$ is the partition coefficient of the permeating solute in the SC (relative to an aqueous solution "w" at a prescribed pH), D_{SC} is its effective diffusivity, and h_{SC} is the total thickness of the SC. Such a decomposition is valid provided that D_{SC} and $K_{\mathrm{SC/w}}$ are determined rigorously as macroscopic outcomes of partitioning and steady state diffusion processes occurring within both lipid and corneocyte phases of the microstructure. As noted above, we make no *a priori* assumptions about the respective roles played by these two phases. Rather, their relative contributions to $(P_{\mathrm{SC/w}})^{\mathrm{comp}}$ emerge naturally as an outcome of the analysis.

Geometry

Key geometrical parameters marked in Figure 1 are the length L of a corneocyte seen in cross section, the corneocyte thickness t, the thickness s of the lipid phase between corneocytes, and the angular parameter φ quantifying how pointed the tips of the corneocytes are. The dashed trapezoid in part c indicates one unit cell, which generates the structure by displacement along integral multiples of the lattice vectors $\mathbf{l}$ and $\mathbf{m}$. The period in the horizontal direction is $l_x = L + s/\sin\varphi$. The thickness of one unit cell in the vertical direction is $m_y = t + s$. For numerical purposes below, it is advantageous to consider an alternate computational domain encompassing the contents of one unit cell, also shown.

Table 2 lists numerical values of all geometrical parameters for the two idealized states of hydration. Values of L, t, and φ derive from a comprehensive analysis of SC microstructure,[54] and are consistent with dimensions assumed by other authors.[24,32,44,47–49] The number n_{b} of bilayers between corneocytes varies considerably, typically from 3 to 9; we take $n_{\mathrm{b}} = 6$ as a reasonable average value. Each bilayer has a thickness δ, for which the best estimate is about 13 nm.[68] Lipid layers

Table 2. Parameters Defining the Model Geometry

(a) Lengths, Thicknesses, Angular Parameter φ, and Tortuosity Parameters

State of SC	L (μm)	t (μm)	s (μm)	φ (°)	τ	ω
Unswollen (partially hydrated)	30.00	0.80	0.091	20	9.66	0.20
Swollen (fully hydrated)	31.20	2.80	0.091	50	3.38	0.19

State of SC	L_1 (μm)	L_2 (μm)	L_3 (μm)	L_1' (μm)	L_2' (μm)	L_3' (μm)
Unswollen (partially hydrated)	1.30	12.13	6.00	1.17	12.13	5.48
Swollen (fully hydrated)	1.89	12.66	6.00	1.83	12.64	5.80

(b) Lattice Vectors

State of SC	$\mathbf{l} = l_x\mathbf{i} + 0\mathbf{j}$ (μm)	$\mathbf{m} = m_x\mathbf{i} + m_y\mathbf{j}$ (μm)
Unswollen (partially hydrated)	30.266066 **i**	(−3.551998) **i** + 0.891000 **j**
Swollen (fully hydrated)	31.318792 **i**	(−3.574163) **i** + 2.891000 **j**

associated with cornified cell envelopes surrounding the corneocytes[43] also contribute to s, each such layer being roughly equivalent to half a bilayer. Thus, altogether, $s = (6 + 0.5 + 0.5)\ \delta = 7\ \delta = 91$ nm. This value agrees well with values for the thickness of the lipid phase assumed in other modeling studies (e.g., 75 nm[24] or 100 nm[32]).

The symbols L_1, L_2, and L_3 represent the lengths of horizontal and diagonal lipid segments within the computational domain. The amount of lateral shift between adjacent corneocyte layers is quantified by L_3 expressed in terms of a fraction $\omega = L_3/l_x$, equal to approximately 0.2 for human skin[54] (see Tab. 2). It determines the geometrical tortuosity factor τ of the lipid pathway as seen in cross section, defined as the ratio of the shortest path length through one corneocyte layer $(2L_1 + L_3)$ to the thickness of this layer $(t + s)$. Based on the formula

$$\tau = \frac{(t+s)/\sin\varphi + \omega(L + s/\sin\varphi)}{t+s}, \qquad (4)$$

it equals 9.7 and 3.4 for partially and fully hydrated skin, respectively. These values are consistent with other quantitative determinations of tortuosity.[24,53,69] Figure 1a and b are drawn to scale and accurately reflect the assumed tortuosity factor.

Shown in Figure 1d is the labeling scheme used to identify individual lipid bilayers and corneocytes within a unit cell. Corneocytes are numbered with a digit running from 1 to 4. Bilayers are indexed using two digits and a letter. The first digit indicates the nearest corneocyte (1, 2, 3, or 4). The second digit indicates the bilayer region (1 for the "L_1" region, etc.). The letter distinguishes among the three neighboring bilayers with the same preceding two digits; it is "a" for bilayers adjacent to the corneocytes. A typical such three-character index (e.g., "12a") is denoted simply as i for brevity in subsequent equations. We tacitly regard i as increasing in passing among bilayers from top to bottom (as drawn in Fig. 2) or from left to right.

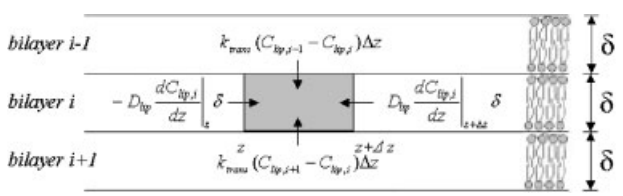

Figure 2. Solute material balance for a segment of a lipid bilayer having length Δz.

Effective Partition Coefficient $K_{SC/w}$

The idealized periodic structure just introduced is imbued with effective properties characterizing its average macroscopic behavior when considered on a length scale large compared with the size of an individual unit cell (or corneocyte). Macroscopically observable affinity of any given solute for the SC is quantified by a partition coefficient $K_{SC/w}$ representing the ratio of superficial solute concentration in the SC (total moles per total volume, accounting for occupancy of both lipid and corneocyte phases by the solute) relative to the concentration in an adjacent aqueous solution (at a prescribed pH) at equilibrium. It is given by the volume average[51,54,70]

$$K_{SC/w} = \phi_{lip} K_{lip/w} + \phi_{cor} K_{cor/w} \qquad (5)$$

where ϕ_{lip} and ϕ_{cor} denote the volume fractions of the lipid and corneocyte phases, respectively. According to Figure 1c

$$\begin{aligned} \phi_{lip} = 1 - \phi_{cor} &= \left(\frac{s}{t+s}\right) \times \frac{L + (s+t)/\sin\varphi}{L + s/\sin\varphi} \\ &= 0.0352 \qquad \text{(for fully hydrated SC)} \\ &= 0.1100 \qquad \text{(for partially hydrated SC).} \end{aligned} \qquad (6)$$

The numerical values follow from the specific dimensions listed in Table 2. They are consistent with typical measured values of SC lipid content (see Tab. 1 of Ref. 70).

The partition coefficient $K_{SC/w}$ is directly applicable to determining SC concentration in equilibrium with an aqueous vehicle. Equilibrium partitioning into the SC from any other vehicle (v, say) would be described by a partition coefficient $K_{SC/v}$ given as the ratio

$$K_{SC/v} = \frac{K_{SC/w}}{K_{v/w}}. \qquad (7)$$

Governing Equations of Transport

Solute motion through the SC is modeled in terms of transport equations containing well-defined lipid- and corneocyte-phase diffusivities and/or mass transfer coefficients. Exchange between these phases involves a partition coefficient reflecting differences in solute affinity between them.

Lipid-Phase Transport

Transport within the lipid phase occurs by lateral diffusion within the plane of any individual

bilayer, and by transfer between bilayers. Significant microscopic modeling work has elucidated the dependence of physicochemical properties and solute concentrations upon position within the bilayer, and shows complex spatial variations in solute energy and mobility.[71–73] In gross terms, three types of zones distinguish themselves:[71] a "relatively large free volume zone around the end of an aliphatic chain" in the middle, "polar headgroup" zones at the edges, and transitional "relatively tight hydrocarbon chain" zones in between (Ref. 71, p 1793; cf. a similar four-zone model[72]). At least for small solutes, transbilayer transport from one bilayer to the next tends to be limited by the rate of permeation between adjacent chains in the transitional tight hydrocarbon zones by a kink shift ("Haines-Liebovich[74]-Träuble[75]") mechanism.[71] We idealize the solute distribution within the lipid phase in terms of effectively one-dimensional distributions of concentration $C_{\mathrm{lip},i}$ representing averages over the cross section of each bilayer i. Each concentration field $C_{\mathrm{lip},i}$ is considered to be a function of a position coordinate "z" running along the bilayer, either parallel to the x axis or along a line of slope tan φ. In the "L_2" and "L_3" regions of Figure 1c, z is essentially synonymous with x.

Solute flux along a bilayer is quantified by Fick's law expressed in terms of a lateral diffusion coefficient D_{lip}:[24,76,77]

$$J_{\mathrm{lat}} = -D_{\mathrm{lip}} dC_{\mathrm{lip},i}/dz. \tag{8}$$

The corresponding molecular flow (moles/time, per unit depth into the page) across a rectangular element of area, perpendicular to and spanning the bilayer at a given value of z, is $J_{\mathrm{lat}}|_z\ \delta$ (see Fig. 2). Solute flux from a bilayer i to an adjacent bilayer $i+1$ (or, equally well, $i-1$) is quantified in a discrete way in terms of a mass transfer coefficient k_{trans} representing the proportionality between this flux and the concentration difference that drives it:[24]

$$J_{\mathrm{trans},i\rightarrow i+1} = k_{\mathrm{trans}}(C_{\mathrm{lip},i} - C_{\mathrm{lip},i+1}). \tag{9}$$

Indices i and $i+1$ could, for instance, represent "12a" and "12b." The molecular flow (moles/time, per unit depth into the page) across a rectangular element of area, separating two bilayers and having length Δz, is $J_{\mathrm{trans}}\ \Delta z$ (see Fig. 2). The discrete treatment of transbilayer movement of solute ("transfer," "hopping") in terms of a mass transfer coefficient (Eq. 9) differs from the continuous treatment of lateral motion in terms of a diffusion coefficient (Eq. 8). The discrete approach to transbilayer transport is commonly used,[24] and appropriate to the approximate level of description employed here, involving effectively one-dimensional longitudinal distributions of solute along a bilayer.

Figure 2 illustrates a material balance over an element of a bilayer i of length Δz: $\Delta z \times (J_{\mathrm{trans},i+1\rightarrow i} + J_{\mathrm{trans},i-1\rightarrow i}) + \delta(J_{\mathrm{lat}}|_z - J_{\mathrm{lat}}|_{z+\Delta z}) = 0$, which expresses the requirement of zero net influx (accumulation) of solute at steady state. In the limit as $\Delta z \rightarrow 0$, this material balance yields the basic bilayer transport equation

$$\frac{d^2 C_{\mathrm{lip},i}}{dz^2} + \frac{k_{\mathrm{trans}}}{\delta D_{\mathrm{lip}}}(C_{\mathrm{lip},i+1} - 2C_{\mathrm{lip},i} + C_{\mathrm{lip},i-1}) = 0. \tag{10}$$

Transbilayer mobility is generally much smaller than lateral mobility, which makes the second (effective source) term a small perturbation of the first (lateral (z-directed) diffusion) term. Technically, Eq. 10 as written is exact for the horizontal bilayers in the "L_2" and "L_3" regions of Figure 1c, and a good approximation for the slanted bilayers in the "L_1" regions. This mathematical point is discussed in the Supplementary Material for this article.

Corneocyte-Phase Transport

Corneocytes are permeable in principle, and their permeability represents a phenomenon likely to be significant at least for relatively hydrophilic compounds. The mere fact of corneocyte swelling on hydration makes it obvious that at least some compounds (water in particular) make it inside. We regard the corneocyte interior as a homogenous, isotropic effective medium, within which solute flux is given by Fick's law

$$\mathbf{J}_{\mathrm{cor}} = -D_{\mathrm{cor}} \nabla C_{\mathrm{cor}} \tag{11}$$

and solute transport is governed by the diffusion equation

$$D_{\mathrm{cor}}\left(\frac{\partial^2 C_{\mathrm{cor}}}{\partial x^2} + \frac{\partial^2 C_{\mathrm{cor}}}{\partial y^2}\right) = 0. \tag{12}$$

In writing equations involving the corneocyte phase, we suppress for brevity the index (1, 2, 3, or 4) on the concentration variable C_{cor}.

It is worth noting that, throughout our analysis, C_{cor} is reckoned as a superficial concentration (total moles of solute per total volume), even though part of the corneocyte ultrastructure (namely the excluded volume associated with

keratin filaments) is inaccessible to the solute at each locale (x, y). All physicochemical parameters related to the corneocyte phase, discussed subsequently, are defined with reference to this understanding for C_{cor}.

Interphase Transport

Corneocytes are surrounded by a cornified cell envelope about 15 nm thick.[78] Although it comprises a denser (and likely less permeable) material than the corneocyte interior, it also constitutes only ~4% of the total thickness of corneocytes. Its attributes of mechanical strength and chemical resistance[78] do not necessarily imply any barrier properties. Indeed, Kasting et al.[79] drew the conclusion that it is not a substantial barrier for water transport from a careful analysis of water mobility in the SC. In view of the preceding facts, we speculate generally that the cell envelope likely offers a resistance to mass transfer that is small relative to the diffusional resistance of the much thicker bulk corneocyte phase. With this assumption, a partitioning equilibrium obtains at the corneocyte-lipid interface to good approximation.

There exists a layer of α-hydroxy ceramides with lipid tails covalently bound (esterified) to the cell envelope, and headgroups apposed to the headgroups of the first lipid bilayer (progressing away from the corneocyte).[29,43,78,80] This lipid monolayer is roughly equivalent to half of one of the true intercellular bilayers, and is here regarded as such. To account for it, we introduce a concentration field $C_{\mathrm{lip},j}$ defined as a function of z in the manner of the lipid bilayer concentrations. (The three-character index j for one of these lipid monolayers linked to the cornified cell envelope ends with the letter "e" for "envelope lipid.") The envelope-lipid concentration $C_{\mathrm{lip},j}$ plays the role of an intermediary between the corneocyte- and lipid-phase concentrations. We note for completeness that, for bilayers adjacent to the corneocytes (for which the three-character index i ends with an "a"), one of the concentrations $C_{\mathrm{lip},i+1}$ or $C_{\mathrm{lip},i-1}$ in Eq. 10 refers to an envelope-lipid layer (for which the three-character j index ends with an "e").

The aforementioned partitioning equilibrium expresses itself in the form of the interfacial condition[48]

$$C_{\mathrm{lip},j} = K_{\mathrm{lip/cor}} C_{\mathrm{cor}} = C_{\mathrm{cor}} / K_{\mathrm{cor/lip}} \qquad (13)$$

in terms of the lipid/corneocyte (or corneocyte/lipid) partition coefficient. Solute conservation at steady state dictates further that solute flux normally out of the corneocyte phase (by diffusion) equal the corresponding flux into the adjacent lipid bilayer i (by the transbilayer hopping mechanism of Eq. 9), lest the envelope-lipid monolayer j between them accumulate solute. Thus,

$$\begin{aligned} \mathbf{n} \cdot (-D_{\mathrm{cor}} \nabla C_{\mathrm{cor}}) &= -\mathbf{n} \cdot D_{\mathrm{cor}} \nabla C_{\mathrm{cor}} \\ &= k_{\mathrm{trans}} (C_{\mathrm{lip},j} - C_{\mathrm{lip},i}) \end{aligned} \qquad (14)$$

where $\mathbf{n}$ denotes the unit normal vector pointing perpendicularly out of the corneocyte phase.

Topology of the Lipid Phase, and Treatment of Corneocyte Tips

Lateral diffusion has been emphasized in the literature as a dominant transport mechanism,[24,76] and it is possible to formulate an idealized topology of the intercellular lipid admitting bilayers that continue indefinitely from unit cell to unit cell without interruption ("Model 1," Fig. 3a). Alternately, each corneocyte might be completely surrounded by intact lipid bilayers ("Model 2," Fig. 3b). In the latter case, progress from one layer of corneocytes to the next requires a transbilayer transport step. To date, brick and mortar models incorporating anisotropy of lipid-phase transport[24] have tacitly assumed Model 1-type behavior. Theories representing the intercellular lipid as an isotropic medium[32,44,46,48–50] do not contain enough physics to effectively distinguish the two scenarios. It is, however, important to keep the question open in principle, and to explore the consequences of different bilayer arrangements. Our Models 1 and 2 can be regarded as idealizations of significant extremes among possible types of lipid-phase structure and connectivity. As such, they likely bracket the real situation. The formulation of a model with the specific purpose of allowing *a priori* a connected path involving only lateral diffusion would be partly biased and contrived.

Any one-dimensional characterization of bilayers necessarily breaks down within the shaded boxes in Figure 1c (which have $O(1)$ aspect ratios) near the tips of the corneocytes (see Fig. 4). The transport Eq. 10 is applied explicitly only in the lipid regions external to these boxes. Thus, lateral diffusion occurs over slightly reduced diffusional path lengths L_1', L_2', and L_3' included in Table 2.[54] Within the shaded boxes, path lengths for lateral diffusion and interfacial areas (per unit depth into the page) for transbilayer transport are

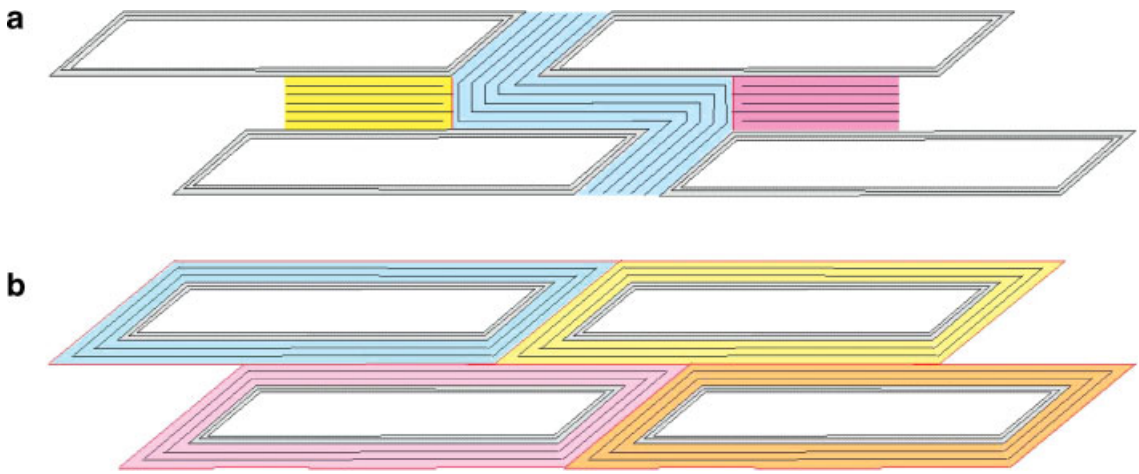

Figure 3. Alternative topologies of the intercellular lipid phase. (a) Model 1, admitting bilayers that continue indefinitely from unit cell to unit cell without interruption. (b) Model 2, in which each corneocyte is completely surrounded by intact lipid bilayers; here progress from one layer of corneocytes to the next requires transbilayer transport steps.

small ($O(s)$). This fact has two consequences. First, the mass transfer resistance for lateral diffusion within the boxes is negligible relative to that associated with the much larger distances L_1', L_2', and L_3'. We therefore regard the boxes to be effectively well mixed in the sense that $C_{\mathrm{lip},i}$ is independent of z there. It is worth stressing that the term "well mixed" refers to a single bilayer, and generally does not imply equality of concentrations among different bilayers. Second, since transbilayer transport is generally significantly slower than lateral diffusion, we in fact usually neglect solute exchange between bilayers within the shaded boxes, given the small $O(s)$ (per unit depth into the page) interfacial areas involved. The Supplementary Material for this article presents in detail the equations that express these considerations mathematically, and serve to link solute concentrations at the termini of different lipid segments separated by the shaded boxes.

Figure 3 is obviously stylized, and is presented solely as a logical and notational reference point. Its presentation, as well as mathematical details in the Supplementary Material required for well-posedness of the unit-cell diffusion problem, do not imply literal belief in the structures shown. Local variations in composition (e.g., cholesterol content) and structure, as well as disordered regions, are likely to exist. More importantly, lipid bilayers bend with a finite radius of curvature as opposed to corners, which would be precluded by a high energy penalty, especially in the case of Model 1. Our purpose in introducing this model is to link up with past work[24] tacitly assuming the existence of bilayers that continue indefinitely from unit cell to unit cell without interruption. Indeed, the same logical difficulties near the corneocyte tips exist there,[24] but appear not to because they are simply not addressed. Our case is strengthened by the finding (see asymptotic analysis for cases where $R >> 1$ below) that the predicted SC permeability is insensitive to the assumed corneocyte tip-related topological details in the common circumstance where the lipid phase is cross-sectionally well mixed.

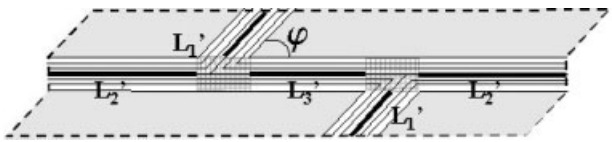

Figure 4. Actual path lengths for lateral lipid-phase diffusion in the model, excluding the corneocyte tip regions.

Effective Diffusivity D_{SC}

Macroscopically observable transport in the y (transdermal) direction is quantified by an effective diffusivity D_{SC}, determined using general theory for diffusion through media with spatially periodic microstructure.[56–58] We use a steady state formalism here in developing the prescription for calculating D_{SC}. The overall idea is to calculate the transdermal ($-y$-directed) solute flux resulting from the imposition of a y-directed solute concentration gradient. This procedure then yields D_{SC} as minus the proportionality

 DOI 10.1002/jps

between flux and concentration gradient. Although the full analysis, presented by Wang,[54] involves a tensor effective diffusivity, the actual set of equations needed to calculate the scalar coefficient D_{SC} can be expressed entirely in terms of scalar quantities.

Notation

For convenience we introduce the symbol $K_{/w}(\mathbf{x})$ to denote the piecewise constant, spatially periodic function of position equal to the partition coefficient $K_{\alpha/w}$ (referred to aqueous solution "w" at a prescribed pH) for positions $\mathbf{x}=(x,y)$ lying in phase α (lipid or corneocyte). Thus, $K_{/w}(\mathbf{x})$ equals either $K_{lip/w}$ or $K_{cor/w}$ at each point $\mathbf{x}$. This function is equivalent to a Boltzmann distribution $\exp[-\Psi(\mathbf{x})/k_BT]$ (or $\exp(-\phi)$ in the notation of Jackson and Coriell[56]) based on the energy Ψ of a solute molecule at each position $\mathbf{x}$, with the convention that the energy Ψ is taken to be zero in aqueous solution. A similar symbol $K_{/lip}(\mathbf{x})$ represents the piecewise constant function of position equal to the partition coefficient $K_{\alpha/lip}$ (referred to SC lipid) for positions $\mathbf{x}=(x,y)$ lying in phase α. Values of $K_{\alpha/lip}$ can be computed from partition coefficients referred to water as the ratio $K_{\alpha/w}/K_{lip/w}$.

We also introduce the collective symbol $C(\mathbf{x})$ to represent the solute concentration at each point. Thus, $C(\mathbf{x})$ equals one of the lipid-phase concentrations $C_{lip,i}(z)$ or corneocyte-phase concentrations $C_{cor}(\mathbf{x})$ for positions $\mathbf{x}$ respectively lying within lipid layer i or within a corneocyte.

Concentration Gradient

We consider the diffusion problem embodied in the preceding lipid- and corneocyte-phase transport equations (Eqs. 10, 12–14) subject to the periodicity conditions

$$C(\mathbf{x}+\mathbf{l})=C(\mathbf{x}), \tag{15}$$

$$C(\mathbf{x}+\mathbf{m})=C(\mathbf{x})+K_{/lip}(\mathbf{x}), \tag{16}$$

which correspond to a macroscopically linear variation in volume-average concentration possessing a gradient with y component[54]

$$\overline{\partial C/\partial y}=\frac{K_{SC/w}}{K_{lip/w}m_y} \tag{17}$$

in which m_y denotes the y component of the lattice vector $\mathbf{m}$ (which equals the vertical thickness of one unit cell). With reference to the unit-cell domain of Figure 1c, the content of Eqs. 15 and 16 is that: (i) C is larger by $K_{/lip}(\mathbf{x})$ (i.e., by unity in the lipid phase and by $K_{cor/lip}=1/K_{lip/cor}$ in the corneocyte phase) and $\partial C/\partial y$ is the same, comparing any point on the top boundary with the equivalent point on the bottom boundary; and (ii) C and $\partial C/\partial x$ are the same, comparing any point on the right boundary with the equivalent point on the left boundary. (The stated partial derivatives can actually be replaced by any oblique derivatives taken in a direction not parallel to the boundary.)

This unit-cell problem determines the solute concentration $C(\mathbf{x})$ uniquely to within an arbitrary multiple of an equilibrium (Boltzmann) distribution. In other words, if $C(\mathbf{x})$ is a solution of these equations, then so is $C(\mathbf{x})+(\text{const})_{/w}\times K_{/w}(\mathbf{x})$ for any value of $(\text{const})_{/w}$ (or, equivalently, $C(\mathbf{x})+(\text{const})_{/lip}\times K_{/lip}(\mathbf{x})$ for any value of $(\text{const})_{/lip}$). This is a well-known (and nonproblematical) feature of the present type of periodic boundary value problem.[57,58] The added multiple of $K_{/w}(\mathbf{x})$ (or $K_{/lip}(\mathbf{x})$) is of no consequence for the calculation of D_{SC} because it generates zero additional flux. (The preceding mathematical statements are technically valid only if the diffusivity is independent of solute concentration, as has been tacitly assumed here.) For definiteness in the numerical calculations reported below, a unique solution is singled out by defining $C(\mathbf{x})$ to be zero at an arbitrarily selected point $\mathbf{x}_0$ within one unit cell, that is, by imposing a requirement of the form

$$C(\mathbf{x}_0)=0. \tag{18}$$

Flux

Of primary interest for SC permeation is the macroscopically observable solute flux in the $-y$ direction, $\overline{J_{-y}}=-\overline{J_y}$, given by the average of the corresponding microscopic (position-dependent) flux over any horizontal line segment spanning the unit cell.[56] Within the framework of Figure 1c, a horizontal line segment convenient for computational purposes is that at the top of the unit cell (at $y=(t+s)/2=L_1\sin\varphi$), which crosses both corneocyte and lipid domains. With all quantities tacitly assumed to be evaluated at this y coordinate (or the corresponding value of z), the average flux is therefore calculated according to the equation

$$\overline{J_{-y}}=\frac{1}{l_x}\left[\int D_{cor}\left(\frac{\partial C_{cor}}{\partial y}\right)dx+\delta D_{lip}\sum\nolimits_{i=1\ldots6}\frac{dC_{lip,i}}{dz}\right]. \tag{19}$$

The corneocyte-phase integral must be evaluated in two parts because the x interval is interrupted by the "L_1" lipid segment. The summation over i refers to the six true lipid bilayers in this "L_1" lipid segment between corneocytes. The Supplementary Material contains some technical remarks regarding this equation.

Effective Diffusivity

The effective diffusivity D_{SC} is minus the constant of proportionality between the macroscopically observable solute flux (Eq. 19) and the macroscopically observable concentration gradient driving the flux (Eq. 17):

$$D_{SC} = \overline{J_{-y}}/\overline{\partial C/\partial y} = \overline{J_{-y}} K_{lip/w} m_y / K_{SC/w}. \quad (20)$$

It is a feature of the assumed geometry, involving nonrectangular unit cells, that a y-directed concentration gradient generally produces a small x-directed flux. This fact is insignificant, because the assumed structure (Fig. 1 et seq.) can be regarded as representative of a local domain of SC tissue, and domains where the corneocytes slant to the right and to the left would arise in equal numbers. Indeed, random anisotropies in real SC are likely to produce small local lateral fluxes, which do not have significance for the question of transdermal permeation. Larger lateral fluxes could, of course, be generated at the boundary of a chemical contact area on the skin, but these are not the subject of the present discussion.

Permeability Coefficient $(P_{SC/w})^{comp}$

Based on the preceding outcomes for $K_{SC/w}$ (Eq. 5) and D_{SC} (Eq. 20), the permeability coefficient of the SC is given by

$$(P_{SC/w})^{comp} = D_{SC} K_{SC/w}/h_{SC} = K_{lip/w}\overline{J_{-y}}/N_{layer} \quad (21)$$

(cf. Eq. 3) where $h_{SC} = N_{layer} m_y = N_{layer}(t+s) = 15(t+s)$ is the total SC thickness. As indicated by the subscript "/w," this coefficient represents the proportionality between solute flux through the SC and a concentration difference imposed across it when the solutions on both sides are aqueous. The permeability coefficient applicable to any other vehicle (v, say) would be

$$(P_{SC/v})^{comp} = \frac{(P_{SC/w})^{comp}}{K_{v/w}} \quad (22)$$

(cf. Eq. 7).

Resumé of Physicochemical Inputs

It is worthwhile to summarize the physicochemical parameters arising in the transport equations formulated above. They are: (i) the partition coefficients $K_{lip/w}$ and $K_{cor/w}$ (defined relative to an aqueous solution "w" at a prescribed pH) for solute in the lipid and corneocyte phases (dimensionless); (ii) the lateral diffusivity for solute motion in the plane of a lipid bilayer (D_{lip}, cm^2/s); (iii) the transbilayer mass transfer coefficient (k_{trans}, cm/s); and (iv) the corneocyte-phase diffusivity (D_{cor}, cm^2/s). Some of these parameters have been measured, others are unknown but measurable in principle, and still others would be difficult to determine directly. It is generally unrealistic to expect values of all parameters to be available for any specific permeating molecule, now or in the near future. Thus, it is essential to develop procedures for physicochemical parameter estimation, working from experimental data as much as possible, and drawing upon theory to fill in gaps in empirical knowledge. This task is undertaken in a separate analysis[70] of SC/water partition coefficients, and in the companion study to this one,[55] which apples the present model to a large SC permeability database. For the moment we regard all diffusion and partition coefficients to be known in principle, and supply values as needed in the illustrative examples presented later. It is worth emphasizing that all physicochemical properties of the corneocyte phase (in particular $K_{cor/w}$ and D_{cor}) are defined with respect to the understanding of C_{cor} as a local superficial concentration (total moles of solute per total volume of the ultrastructure).

Effects of Hydration

Within the framework established above, hydration affects SC permeability in two ways. Swelling of corneocytes causes a very obvious change in microscopic geometry, represented quantitatively in Figure 1a and b. The increase in thickness alone would generally decrease permeability, although—as discussed in the Results below—under certain well-defined circumstances this geometrical change has little or no quantitative effect on the overall permeability.

Hydration has the further effect of generally increasing D_{lip}, D_{cor}, and $K_{cor/w}$ for any given solute. Increases in D_{lip}[29,68,79] are commonly identified with disordering of lipid chains by water molecules and/or straining caused by swelling of

the corneocytes. Values of $K_{lip/w}$ could also be affected by such structural changes, although the effect is likely to be less dramatic. Increases in D_{cor} and $K_{cor/w}$ are understandable from a view of the corneocyte interior phase as a composite material comprising keratin microfibrils embedded within a connected surrounding aqueous phase.[54,55] The fractional volume excluded by the keratin decreases as the water fraction increases, making more of the total volume accessible to a permeating solute (thereby increasing $K_{cor/w}$), and decreasing the obstacle/tortuosity and hydrodynamic hindrance factors for diffusion (increasing D_{cor}).

The slanted bilayers in the "L_1" lipid segment would technically have to undergo stretching in the hydration process. We do not attempt a literal description of this process, and simply consider partially and fully hydrated states of the SC to have equilibrated microstructures in which the lipid phase is organized into parallel bilayers. The larger value of D_{lip} characterizing the fully hydrated state does, however, offer some representation of possible effects of disordering and/or straining caused by corneocyte swelling.

Possible Effects of Keratin Binding

Retinyl ascorbate, for example, is known to bind to keratin.[81] Water itself binds significantly to keratin,[61,79,82] although this case represents an exceptional situation (water self-dffusion). Binding to keratin protein (or other material associated with the corneocytes, for example, cornified cell envelope proteins and lipid) has, in fact, been well documented for a variety of other solutes,[35,37,43,81] and quantified in terms of an effective partition coefficient correlated with $K_{o/w}$.[35,70] This phenomenon increases holdup of solute in the corneocyte phase, thereby increasing $K_{cor/w}$. It concomitantly slows diffusion (i.e., decreases D_{cor} if D_{cor} is taken to describe all (bound and free, not just free) solute) because solute is immobile in its bound state.

The effects of increased holdup and decreased mobility tend to cancel in the permeability coefficient $(P_{SC/w})^{comp}$. Indeed, at low solute concentrations binding can be described by a partition coefficient (or linear isotherm).[35,37,43] In this limit the product $K_{cor}D_{cor}$, representing corneocyte permeability, is not affected by binding, even though the individual factors are.[54,55] As is evident in the next section, only the product $K_{cor}D_{cor}$ enters the calculation of $(P_{SC/w})^{comp}$.

Dimensionless Formulation and Key Dimensionless Groups

It is advantageous to introduce a dimensionless formulation of the preceding governing equations, because such a formulation reveals the key dimensionless groups determining SC permeability. To avoid purely cosmetic restatements, attention is restricted here to only the most crucial equations that reveal these groups.

The nondimensionalization process is started by dividing all position coordinates and length parameters by a characteristic length representative of the spatial scale of variations in solute concentration. A suitable choice is the period of the model microstructure in the x direction, l_x. Dimensionless quantities are distinguished by attaching the "hat" (^) affix to the symbol for the corresponding dimensional quantity. Thus, we introduce new coordinates $\hat{x} = x/l_x,\ \hat{y} = y/l_x,\ \hat{z} = z/l_x,$ lengths $\hat{s} = s/l_x, \hat{t} = t/l_x, \hat{L} = L/l_x$, etc., and lattice vectors $\hat{\mathbf{l}} = (l_x)^{-1}\,\mathbf{l}$, $\hat{\mathbf{m}} = (l_x)^{-1}\,\mathbf{m}$. The dimensionless thickness of one unit cell in the vertical direction is the y component of $\hat{\mathbf{m}}$, $\hat{m}_y = m_y/l_x$.

The notation $\hat{C}$ is used to indicate solute concentration fields regarded as functions of dimensionless position $\hat{\mathbf{x}} = (\hat{x},\hat{y})$. Thus within the lipid phase

$$\hat{C}_{lip,i}(\hat{z}) = C_{lip,i}(z). \tag{23}$$

Within the corneocyte phase it proves advantageous to define $\hat{C}_{cor}$ to be the lipid-equivalent concentration

$$\hat{C}_{cor}(\hat{\mathbf{x}}) = C_{cor}(\mathbf{x})K_{lip/cor} = C_{cor}(\mathbf{x})/K_{cor/lip}. \tag{24}$$

Partitioning equilibria at lipid-corneocyte interfaces (Eq. 13) therefore reduce to the equality

$$\hat{C}_{lip,j} = \hat{C}_{cor}. \tag{25}$$

The collective symbol $\hat{C}(\hat{\mathbf{x}})$ represents $\hat{C}_{lip,i}(\hat{z})$ within the lipid phase and $\hat{C}_{cor}(\hat{\mathbf{x}})$ within the corneocyte phase. In terms of previously introduced notation, it is technically correct to write

$$\hat{C}(\hat{\mathbf{x}}) = C(\mathbf{x})/K_{/lip}(\mathbf{x}). \tag{26}$$

This new concentration field is a continuous function of position defined over the entire unit cell, suffering no jumps at lipid-corneocyte phase boundaries. The periodicity conditions Eqs. 15 and 16 adopt the simple form

$$\hat{C}(\hat{\mathbf{x}} + \hat{\mathbf{l}}) = \hat{C}(\hat{\mathbf{x}}), \tag{27}$$

$$\hat{C}(\hat{\mathbf{x}} + \hat{\mathbf{m}}) = \hat{C}(\hat{\mathbf{x}}) + 1 \tag{28}$$

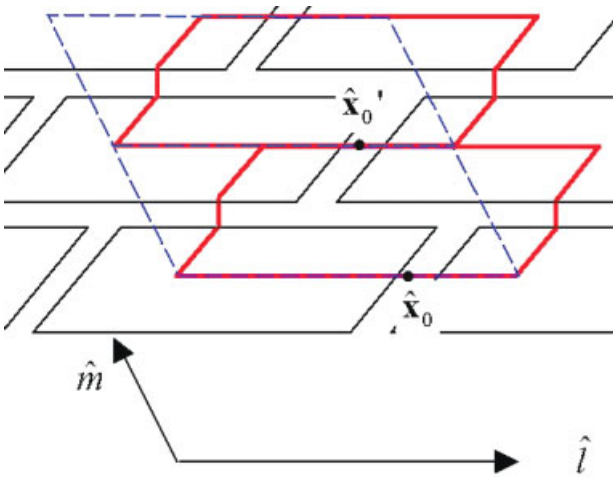

Figure 5. Equivalent points $\hat{\mathbf{x}}_0$ and $\hat{\mathbf{x}}_0'$ at opposite sides of a unit cell.

expressing the fact that $\hat{C}(\hat{\mathbf{x}})$ increases by unity going from any point at the bottom of a unit cell to the equivalent point at the top. A unique solution of the transport equations is specified by requiring that

$$\hat{C}(\hat{\mathbf{x}}_0) = 0, \text{ or } \hat{C}(\hat{\mathbf{x}}_0') = 1, \tag{29}$$

with $\hat{\mathbf{x}}_0$ and $\hat{\mathbf{x}}_0'$ the points marked in Figure 5. The two members of Eq. 29 are equivalent owing to Eq. 28.

In terms of dimensionless variables, the lipid-phase diffusion equation (Eq. 10) expresses itself as

$$\frac{d^2\hat{C}_{\text{lip},i}}{d\hat{z}^2} + \left(\frac{k_{\text{trans}}l_x^2}{D_{\text{lip}}\delta}\right)(\hat{C}_{\text{lip},i+1} - 2\hat{C}_{\text{lip},i} + \hat{C}_{\text{lip},i-1}) = 0. \tag{30}$$

The interfacial condition involving solute flux between lipid and corneocyte phases (Eq. 14) takes the form

$$-\mathbf{n}\cdot\hat{\nabla}\hat{C}_{\text{cor}} = \left(\frac{k_{\text{trans}}l_x}{D_{\text{cor}}K_{\text{cor/lip}}}\right)(\hat{C}_{\text{lip},j} - \hat{C}_{\text{lip},i}) \tag{31}$$

in which $\hat{\nabla} = \mathbf{i}\partial/\partial\hat{x} + \mathbf{j}\partial/\partial\hat{y}$ denotes the dimensionless gradient operator. Of special pertinence to SC permeability is the dimensionless average $-y$-directed component of the solute flux, $\overline{\hat{J}_{-y}} = (l_x/D_{\text{lip}})\overline{J_{-y}}$, given by

$$\overline{\hat{J}_{-y}} = \frac{D_{\text{cor}}K_{\text{cor/lip}}}{D_{\text{lip}}}\int\left(\frac{\partial\hat{C}_{\text{cor}}}{\partial\hat{y}}\right)d\hat{x} + \frac{\delta}{l_x}\sum\nolimits_{i=1\ldots6}\frac{d\hat{C}_{\text{lip},i}}{d\hat{z}} \tag{32}$$

(cf. Eq. 19). In terms of it, the effective SC diffusivity D_{SC} is given by the following version of Eq. 20:

$$\frac{D_{\text{SC}}K_{\text{SC/w}}}{D_{\text{lip}}K_{\text{lip/w}}} = \overline{\hat{J}_{-y}}\hat{m}_y \equiv (\hat{P}_{\text{SC/w}})^{\text{comp}}. \tag{33}$$

Here we have introduced a convenient dimensionless coefficient $(\hat{P}_{\text{SC/w}})^{\text{comp}}$, in terms of which the dimensional SC permeability of ultimate interest is given by

$$(P_{\text{SC/w}})^{\text{comp}} = \frac{(\hat{P}_{\text{SC/w}})^{\text{comp}}D_{\text{lip}}K_{\text{lip/w}}}{h_{\text{SC}}} \tag{34}$$

with h_{SC} the thickness of the stratum corneum.

Equations 30–32 reveal the three key dimensionless groups determining SC permeability (given by Eqs. 32–34). The parameter

$$R \equiv \frac{k_{\text{trans}}l_x^2}{\delta D_{\text{lip}}} = \frac{k_{\text{trans}}l_x}{\delta D_{\text{lip}}/l_x} \tag{35}$$

appearing in Eq. 30 represents a ratio of transbilayer to lateral molecular flows, applicable to a lipid bilayer segment of length l_x and thickness δ, respectively caused by a unit concentration difference. It determines the strength of transbilayer transport acting as an effective source term in this equation. The quantity

$$\hat{\delta} \equiv \frac{\delta}{l_x} \tag{36}$$

is just the aspect ratio of the bilayer segment. These two groups determine the permeability of the lipid pathway through the SC. Since the dimensions δ and l_x are already determined, only the former (R) represents an adjustable parameter.

If a continuous approach to transbilayer transport based on a transverse diffusivity D_{trans} were being used (which is not the case here), then k_{trans} would be roughly identifiable with D_{trans}/δ; equivalently, $D_{\text{trans}} \approx k_{\text{trans}}\,\delta$. The ratio of transverse to lateral diffusivities would then be given by

$$\frac{D_{\text{trans}}}{D_{\text{lip}}} \approx \left(\frac{k_{\text{trans}}l_x^2}{\delta D_{\text{lip}}}\right)\left(\frac{\delta}{l_x}\right)^2 = R\hat{\delta}^2. \tag{37}$$

This relation will allow us to assess later the apparent degree of diffusional anisotropy of the lipid phase.

Equation 32 contains the reciprocal of one further dimensionless group, which comes into play because corneocyte permeability is allowed for in the analysis, namely

$$\sigma \equiv \frac{D_{\text{lip}}K_{\text{lip/cor}}}{D_{\text{cor}}} = \frac{D_{\text{lip}}}{D_{\text{cor}}K_{\text{cor/lip}}} = \frac{D_{\text{lip}}K_{\text{lip/w}}}{D_{\text{cor}}K_{\text{cor/w}}}. \tag{38}$$

 DOI 10.1002/jps

This parameter has been considered in previous analyses[46,49] (also c.f. Refs. 26,44,48,50,51). It is worth noting that lipid- and corneocyte-phase diffusivities and partition coefficients appear in the ratio σ as products $D_\alpha K_{\alpha/w}$, and do not actually enter the analysis separately. In other words, the steady state permeability of a phase α (lipid or corneocyte) is determined by the product of mobility and affinity factors, which are not separately discernible. The group $k_{trans}\, l_x/D_{lip}\, K_{cor/lip}$ appearing in Eq. 31 is nothing other than $R\hat{\delta}\sigma$.

If the SC were a homogeneous lipid membrane with diffusivity D_{lip} and thickness h_{SC}, its permeability would be simply $D_{lip}K_{lip/w}/h_{SC}$. Obviously this value must be corrected to account for several facts. (i) The length of the lipid path greatly exceeds h_{SC}, by tortuosity factors of 9.7 and 3.4 for partially and fully hydrated skin, respectively, based on the assumed geometry (see Tab. 2). (ii) The area fraction $[(s/\sin\varphi)/l_x]$ of the lipid phase in a plane parallel to the skin surface is small (<1%). (iii) Depending on the values of D_{cor}, $K_{cor/w}$, and k_{trans}, intracellular diffusion and transbilayer hopping may play significant additional roles in determining SC permeability. $(\hat{P}_{SC/w})^{comp}$, the key outcome of our model, is the multiplicative factor accounting rigorously for all these phenomena. It multiplies $D_{lip}K_{lip/w}/h_{SC}$ to produce the dimensional permeability $(P_{SC/w})^{comp}$ (see Eq. 34).

METHODS OF SOLUTION

Numerical techniques yield quantitative results for arbitrary values of the physicochemical parameters. Approximate asymptotic solutions can be obtained analytically in certain limiting cases, which yield important physical insights and serve as checks on the numerical analysis.

Numerical Solution

Dimensionless versions of the transport equations (Eqs. 25 and 27–31, together with implied dimensionless statements of all other governing equations) comprise a coupled system of ordinary and partial differential equations generally requiring a numerical solution. Our numerical scheme involves an oblique coordinate system, and solution of finite difference discretizations of these equations on a variable mesh by relaxation. It is described comprehensively by Wang,[54] to which we refer the reader for all details, in the interest of brevity, because they are not strictly required for subsequent discussion.

Asymptotic Analysis

The cases of impermeable corneocytes ($\sigma \to \infty$) and highly permeable corneocytes ($\sigma \to 0$) are both extremes in which asymptotes can be obtained analytically for the dependence of $(\hat{P}_{SC/w})^{comp}$ upon R for $R \gg 1$ and $R \ll 1$. These asymptotes, presented in Table 3, are derived in the Supplementary Material for this article. The derivation reveals interesting phenomena. For instance, for impermeable corneocytes ($\sigma \to \infty$), solute flux arises only from diffusion through the ribbonlike network comprising the lipid phase. In the limit $R \gg 1$ transbilayer hopping is sufficiently fast to render the lipid phase cross-sectionally well mixed. In other words, within any lipid region ("L_1", "L_2", "L_3") all the lipid concentrations $\hat{C}_{lip,i}$ tend to become equal to each other. However, when the corneocytes are highly permeable ($\sigma \to 0$), for $R \gg 1$ the lipid phase is not, in fact, cross-sectionally well mixed, as was the case for impermeable corneocytes. The reason is that the individual bilayer concentrations are now controlled by the corneocyte phase via the lipid/corneocyte phase partitioning equilibrium (see Eqs. 13 and 25), and not the mechanics of lipid-phase diffusion occurring in isolation. The Supplementary Material presents a detailed discussion of these and other points underlying the final results listed in Table 3.

RESULTS

Of central interest is the manner in which the permeability coefficient $(\hat{P}_{SC})^{comp}$ depends upon the key parameters $R = (k_{trans}\ l_x^2)/(\delta\ D_{lip})$ and $\sigma = D_{lip}K_{lip/cor}/D_{cor} = D_{lip}/(D_{cor}K_{cor/lip}) = D_{lip/w}\ K_{lip/w}/(D_{cor}K_{cor/w})$. The former represents a ratio of transbilayer to lateral molecular mobilities in the lipid phase, and the latter represents a ratio of lipid- to corneocyte-phase permeabilities. $(\hat{P}_{SC/w})^{comp}$ is the correction factor that multiplies $D_{lip}K_{lip/w}/h_{SC}$ to produce the dimensional SC permeability $(P_{SC/w})^{comp}$ (see Eq. 34), accounting rigorously for all aspects of the composite microstructure.

Numerical Results

Figures 6 and 7 show the computed dependence of $(\hat{P}_{SC/w})^{comp}$ upon R and σ. A convenient numerical tabulation of the results, suitable for interpolation in the subset of the parameter space most

Table 3. Asymptotes for $(\hat{P}_{SC/w})^{comp}$ for Limiting Values of σ and R

Corneocytes	R	Formula(s)		
Impermeable ($\sigma \to \infty$)	$R \gg 1$	Eq. A and Eq. B with $\alpha = \dfrac{0.5/\hat{L}'_1}{\dfrac{1}{\hat{L}'_1} + \dfrac{R\hat{\delta}(1/\hat{L}'_2)}{R\hat{\delta} + (1/\hat{L}'_2)} + \dfrac{2}{\hat{L}'_3}}$	(Model 1)	Eq. C (or Eq. S17)
		$\alpha = \dfrac{0.5/\hat{L}'_1}{\dfrac{1}{\hat{L}'_1} + \dfrac{1}{\hat{L}'_2} + \dfrac{2}{\hat{L}'_3}}$	(Model 2)	Eq. D (or Eq. S18)
	$R \ll 1$	Eq. A and Eq. B with $\alpha = \dfrac{0.5/\hat{L}'_1}{\dfrac{1}{\hat{L}'_1} + \dfrac{2}{\hat{L}'_3}}$	(Model 1)	Eq. E (or Eq. S17 with $R\hat{\delta} = 0$)
		$(\hat{P}_{SC/w})^{comp} = (2\hat{L}'_2 + \hat{L}'_3)R\hat{\delta}\hat{m}_y$	(Model 2)	Eq. F (or Eq. S20)
Highly permeable ($\sigma \to 0$)	$R \gg 1$	$(\hat{P}_{SC/w})^{comp} = \dfrac{1}{7}(2\hat{L}'_2 + \hat{L}'_3)R\hat{\delta}\hat{m}_y$	(for both Model 1 and Model 2)	Eq. G (or Eq. S21)
	$R \ll 1$	Results are identical to those for the limit $\sigma \to \infty$, $R \ll 1$: Eq. A and Eq. B with α given by Eq. E (for Model 1), and Eq. F (for Model 2)		

Many results refer to the equations

$$(\hat{C}_{lip})_1 = 0.5 + \alpha, \qquad \text{Eq. A (or Eq. S14)}$$

$$(\hat{P}_{SC/w})^{comp} = \overline{\hat{J}_{-y}}\hat{m}_y = \frac{6\hat{\delta}\hat{m}_y[1 - (\hat{C}_{lip})_1]}{\hat{L}'_1}. \qquad \text{Eq. B (or Eq. S16)}$$

The derivation of all formulas is given in the Supplementary Material for this article (numbers preceded by the letter "S" refer to equations appearing therein).

pertinent to experimental reality, is included in the Supplementary Material for this article.

For all values of σ, the different types of lipid-phase topology represented by Models 1 and 2 lead to radically different permeability values for small R, but essentially indistinguishable values for large R. This fact is not surprising in light of the asymptotic analysis (Tab. 3), which yielded this conclusion for the extremes $\sigma \to \infty$ and $\sigma \to 0$. The numerical results at intermediate values of σ follow suit. The underlying physical reason is clear. According to Model 1, $(\hat{P}_{SC/w})^{comp}$ has a minimum value of about 8×10^{-4} (for fully hydrated skin; see Figs. 6a and 7a). No matter how small R (or k_{trans}), the assumed lipid-phase topology guarantees this minimum level of (dimensionless) permeability from a connected pathway traversable by lateral diffusion; $(\hat{P}_{SC/w})^{comp}$ levels off as R decreases. In contrast, according to Model 2, transbilayer hopping is necessary to traverse the SC; $(\hat{P}_{SC})^{comp}$ continually decreases with decreasing R.

It is important to distinguish two related but distinct questions, namely, what is the amount of solute holdup in the corneocyte phase, and what is the degree to which the corneocytes contribute to the total solute flux through the SC? As defined in Eq. 26 above, the dimensionless concentration $\hat{C}(\hat{\mathbf{x}}) = C(\mathbf{x})/K_{/lip}(\mathbf{x})$ represents the lipid-equivalent concentration at each point. It is a continuous function of position (cf. Eq. 25). Within the corneocytes, the true solute concentration is obtained by multiplying the (order unity) field $\hat{C}(\hat{\mathbf{x}})$ by $K_{cor/lip}$ (cf. Eq. 24). The implied corneocyte-phase solute holdup is large or small depending upon the value of $K_{cor/lip}$. Flux through the corneocyte phase depends not upon $K_{cor/lip}$ *per se*, but more precisely upon $K_{cor/lip}$ in combination with D_{cor}, coupled with the large cross-sectional area presented by the corneocytes.

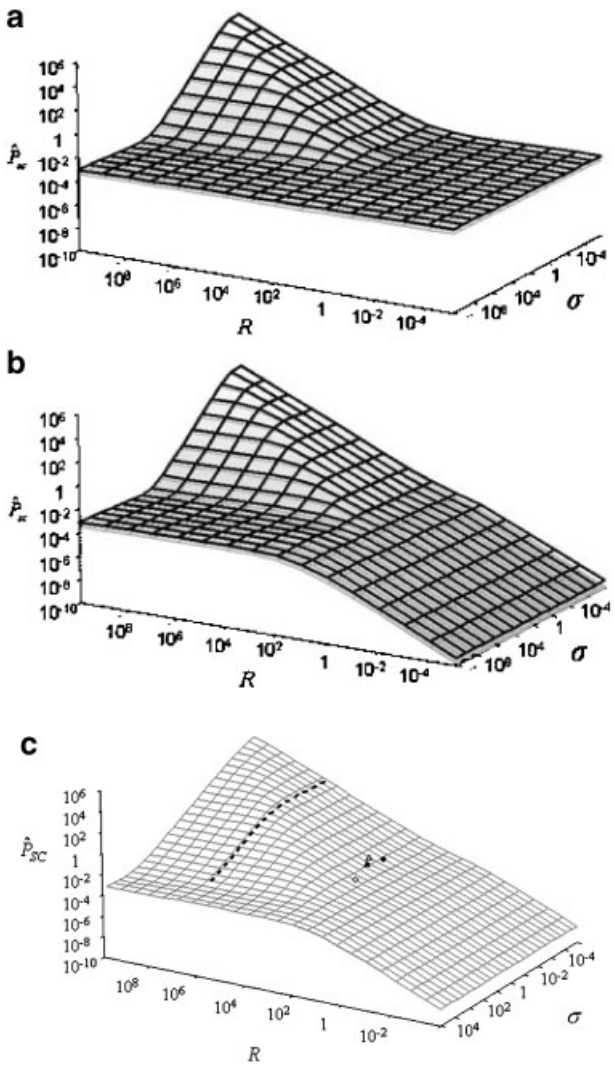

Figure 6. (a, b) Logarithmic plots showing approximately the dependence of $(\hat{P}_{SC/w})^{comp}$ upon R and σ for (a) Model 1 and (b) Model 2. In both these parts, the (upper) surface defined by the mesh of thick lines represents swollen (fully hydrated) SC, and the (lower) gray surface with thin lines represents unswollen (partially hydrated) SC. (c) Detail of the parameter space for Model 2 for swollen (fully hydrated) skin. The positions of four illustrative compounds considered later are marked (△ water, ▲ ethanol, ● nicotinamide, ○ testosterone). The dotted curve marked on the surface represents the section corresponding to isotropic lipid-phase diffusion. Such large values of R are clearly far removed from realistic cases.

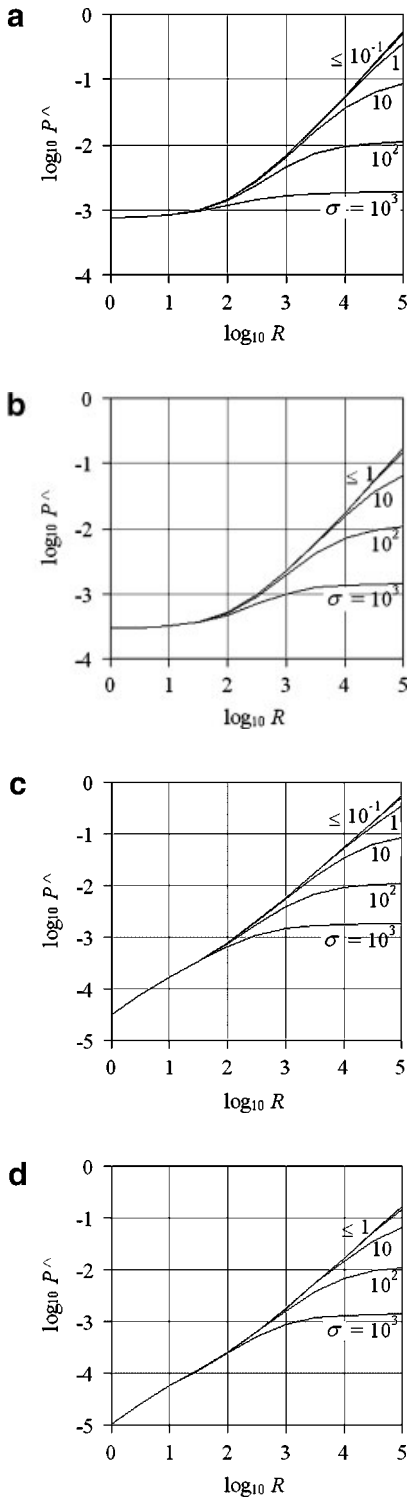

Figure 7. Plots showing the dependence of $\log_{10}(\hat{P}_{SC/w})^{comp}$ upon $\log_{10} R$ at various values σ: (a) Model 1 for swollen (fully hydrated) skin; (b) Model 1 for unswollen (partially hydrated) skin; (c) Model 2 for swollen (fully hydrated) skin; and (d) Model 2 for unswollen (partially hydrated) skin.

It may also be observed in Figures 6 and 7 that corneocyte permeation enhances SC permeability (i.e., $(\hat{P}_{SC/w})^{comp}$ increases with decreasing σ at fixed R) only when R is sufficiently large, greater than about 10^2. The reason is that transcellular transport can enhance SC permeation only when

k_{trans} is sufficiently large. This finding accords with intuition, because motion along the transcellular pathway necessarily involves transbilayer hopping through the intercellular lipid. (At fixed $R > \approx 10^2$, the increase in $(\hat{P}_{SC/w})^{comp}$ with decreasing σ is from a baseline value given by Eqs. A–D in Table 3 ($\approx 8 \times 10^{-4}$ for fully hydrated skin) to an upper plateau of $(2\hat{L}'_2 + \hat{L}'_3)R\hat{\delta}\hat{m}_y/7$ (see Eq. G in Tab. 3).) For smaller values of R, decreasing σ has no effect upon permeability, because motion along the transcellular pathway becomes too limited by the necessary interruption of transbilayer hopping to make a significant contribution to the flux.

For sufficiently large R (again, greater than about 10^2), the relative flux contributions of corneocyte and lipid phases can be estimated very roughly from Eq. 32 without detailed computation. Owing to Eq. 25, the concentration fields $\hat{C}_{cor}$ and $\hat{C}_{lip,i}$ tend to be tied together. Thus, $d\hat{C}_{lip,i}/d\hat{z} \approx (\sin\varphi)\,\partial\hat{C}_{cor}/\partial\hat{y}$. (The factor $\sin\varphi$ arises because the lipid bilayers make an angle φ with the horizontal in the "L_1" lipid segment, as opposed to being vertical). The resulting contributions to $\hat{J}_{-y}$ are determined by their effective multipliers in Eq. 32, which are $1/\sigma = D_{cor}\,K_{cor/lip}/D_{lip}$ and $6\hat{\delta}\sin\varphi = 6\ (\delta/l_x)\ \sin\varphi$, respectively. Therefore, the ratio of lipid- to corneocyte-phase contributions to flux through the SC is of the order of $6\hat{\delta}(\sin\varphi)\sigma$. This ratio establishes an approximate cutoff, $\sigma_{cutoff} \approx 1/(6\hat{\delta}\sin\varphi) \approx 500$ or 1100 for fully or partially hydrated SC, respectively, separating the regimes in which most of the solute travels by lateral diffusion within the intercellular lipid ($\sigma > \sigma_{cutoff}$), and by transcellular diffusion within the corneocytes ($\sigma < \sigma_{cutoff}$). Specific numerical examples of the distribution between computed lipid- and corneocyte-phase contributions to the total flux are presented in Table 4, for values of R typical of real permeants (see examples and Tab. 5 below). For large R the actual numerically determined values of σ_{cutoff} are approximately 1200 and 3400 for fully and partially hydrated SC, respectively. The large magnitude of σ_{cutoff} is primarily a consequence of the small relative width ($6\hat{\delta}$) of the lipid pathway. The concept of σ_{cutoff} loses meaning at small values of R (or k_{trans}). Here the lipid pathway provides the primary route through the SC, irrespective of σ, because (as noted above) motion along the transcellular pathway becomes too strongly limited by the necessary interruption of transbilayer hopping.

Table 4. Distribution Between Lipid- and Corneocyte-Phase Contributions to the Total Flux Through Fully Hydrated SC for Model 2

	Percentage of Total Flux Contributed by Lipid Phase	
σ	$R = 100$	$R = 1000$
1	43.8	8.3
10	44.1	8.9
10^2	46.1	14.9
10^3	59.6	45.4
10^4	88.3	87.9

As stated earlier, major effects of hydration are generally increases in D_{lip}, D_{cor}, and $K_{cor/lip}$, all of which tend to increase SC permeability, and also alter the numerical values of σ and R. Aside from these obvious effects, the change in geometry caused by swelling of the corneocytes can affect the dimensionless flux $\hat{J}_{-y} = (\hat{P}_{SC/w})^{comp}/\hat{m}_y$ even at hypothetically fixed values of σ and R. $\hat{J}_{-y} = (\hat{P}_{SC/w})^{comp}/\hat{m}_y$ (as opposed to just $(\hat{P}_{SC/w})^{comp}$) is the true determinant of the dimensional SC permeability because of the presence of SC thickness ($h_{SC} = N_{layer}\,m_y = N_{layer}\,\hat{m}_y\,l_x$) in the denominator of Eq. 34. For (hypothetically) fixed σ and R, the flux $\hat{J}_{-y}$ is actually insensitive to the geometrical effect of hydration under a number circumstances. For the lipid pathway in Model 1, the "L_1" segments constitute a minority of the total (mostly horizontal) lipid path length, which therefore hardly changes upon swelling. Also, swelling of the corneocytes is clearly irrelevant if they are impermeable to a given solute ($\sigma \to \infty$), and the longer diffusional path through them also has no effect if they are highly permeable (effectively transparent to the solute, $\sigma \to 0$). In general, however, the change in microscopic geometry caused by hydration leads to modest changes in $\hat{J}_{-y}$ (by an $O(1)$ factor) even at (hypothetically) fixed values of σ and R. This phenomenon constitutes a hydration effect additional to the obvious effect of increasing D_{lip}, $D_{cor/lip}$, and $K_{cor/lip}$, which directly affects the factor $D_{lip}K_{lip/w}$ in Eq. 34 and also alters the dimensionless groups σ and R.

Agreement with Theoretical Asymptotes

Figure 8 shows further selected sections of the surfaces represented in Figure 6, namely $(\hat{P}_{SC/w})^{comp}$ as a function of R for $\sigma = 10^6$ ($\log_{10}\ \sigma = 6$) and $\sigma = 10^{-4}$ ($\log_{10}\ \sigma = -4$). The extreme values selected respectively represent the limiting cases of effectively impermeable corneocytes and very highly permeable (effectively "transparent")

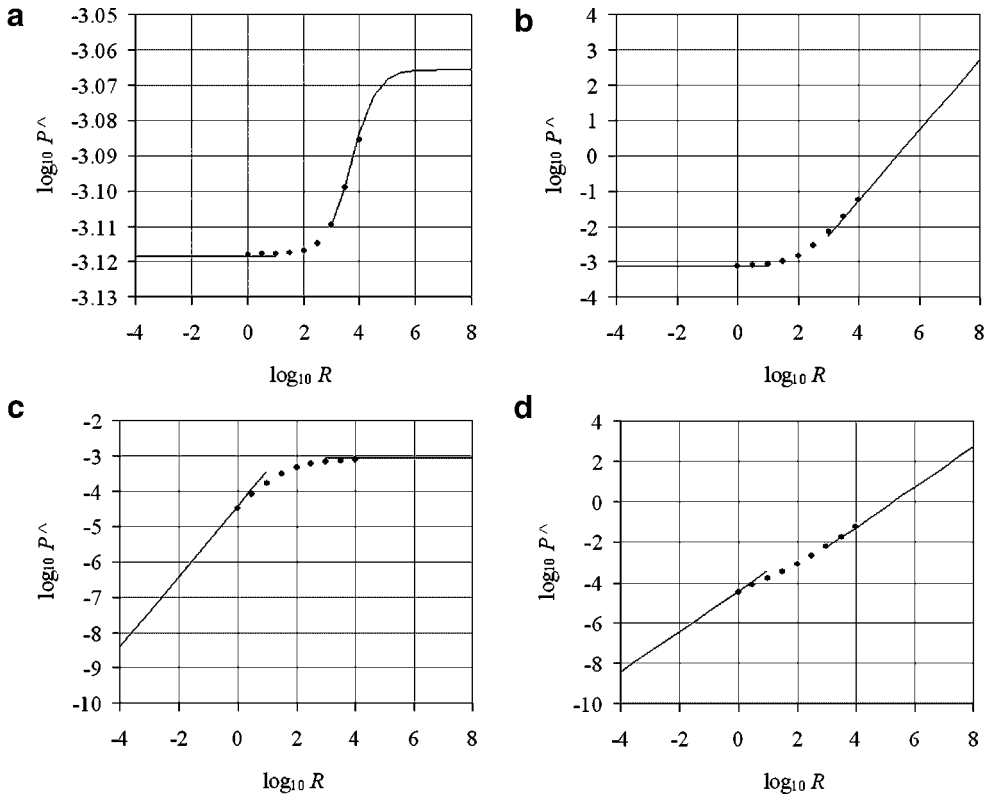

Figure 8. Logarithmic plots showing the dimensionless permeability $(\hat{P}_{SC/w})^{comp}$ as a function of R for $\sigma = 10^6$ ($\log_{10}\sigma = 6$; limiting case of impermeable corneocytes) and $\sigma = 10^{-4}$ ($\log_{10}\sigma = -4$; limiting case of very highly permeable corneocytes): (a) Model 1, $\sigma = 10^6$; (b) Model 1, $\sigma = 10^{-4}$; (c) Model 2, $\sigma = 10^6$; (d) Model 2, $\sigma = 10^{-4}$. Dashed lines represent the asymptotes for $R \ll 1$ and $R \gg 1$ listed in Table 3 for each case. All results shown are for the case of fully hydrated SC.

corneocytes. In each case, for both Model 1 and Model 2, there is excellent agreement between the numerical results for $(\hat{P}_{SC/w})^{comp}$ and the asymptotes derived analytically for $R \gg 1$ and $R \ll 1$ (see Tab. 3). This agreement both supports the veracity of our numerical scheme, and confirms the physical interpretations presented in the asymptotic analysis (see Supplementary Material).

Isotropic Lipid-Phase Diffusion

According to Eq. 37, diffusion in the lipid phase would be isotropic ($D_{trans} \approx D_{lip}$) for the hypothetical value $R = 1/\hat{\delta}^2 \approx 6 \times 10^6$. This value is definitely not typical of reality, because R seems to be considerably smaller (by three to six orders of magnitude) than 6×10^6 for most compounds,[54,55] that is, lipid-phase diffusion is generally markedly anisotropic (see points and dashed line marked in Fig. 6c). Nevertheless, it is worthwhile to discuss briefly the case of isotropic lipid-phase diffusion, because a number of authors[32,44,46,48–50] have based their numerical calculations on this assumption.

In particular, Charalambopoulou et al.[49] developed such a brick-and-mortar model and compared it with Michaels et al.'s[44] and Tojo's[46] models. They chose for their geometrical parameter values $t = 0.8$ μm, $s = 0.07$ μm, and considered two different corneocyte lengths, namely $L = 40$ and 20 μm (as expressed in the present notation). The stacking of their rectangular corneocytes was fully staggered ($\omega = 0.5$). We modified our Model 2 to use the values of L, t, s, and ω employed by Charalambopoulou et al., and also set the angle φ to 90° to match their assumed rectangular corneocyte shape. (The distinction between Models 1 and 2 is actually unimportant here, because they give essentially identical results for $(\hat{P}_{SC/w})^{comp}$ at large values of R). Figure 9 compares the resulting dependencies of $(\hat{P}_{SC/w})^{comp}$ on σ with corresponding results read from Charalambopoulou et al.'s Figure 7. (Charalambopoulou et al.'s effective diffusivity D_{eff} corresponds to $D_{SC}K_{SC/w}/K_{lip/w}$ in

present notation, making their dimensionless abscissa $D_{\text{eff}}/D_{\text{lip}}$ equivalent to our $(\hat{P}_{\text{SC/w}})^{\text{comp}}$.) The good agreement further supports the accuracy of our numerical scheme for the applicable values of R ($R \approx 1.6 \times 10^7$ for $L = 40$ μm and $R \approx 4 \times 10^6$ for $L = 20$ μm). The small discrepancy in the apparent limiting values of $(\hat{P}_{\text{SC/w}})^{\text{comp}}$ as $\sigma \to 0$ may be due to the approximate manner in which transbilayer hopping (with k_{trans} adjusted to make $D_{\text{trans}} \approx D_{\text{lip}}$—cf. Eq. 37) represents truly two-dimensional isotropic diffusion, especially near the corneocyte tips.

Charalambopoulou et al.[49] present a detailed discussion of the shape of the curves in Figure 9. Divergence in the results corresponding to the two choices of L occurs only at large σ, and arises mainly from the difference in tortuosity of the (dominant) intercellular lipid pathway. These authors also compare their model with Michaels et al.'s[44] and Tojo's.[46] The reader is referred to their discussion[49] regarding these points.

Comparison with the Model of Johnson et al. (1997)[24]

Johnson et al.[24] presented a brick-and-mortar analysis that is predicated upon a lipid-phase topology furnishing *a priori* a connected path involving only lateral diffusion, and does not

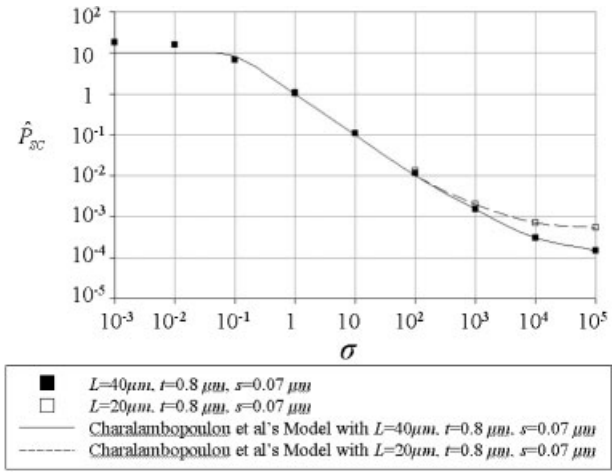

Figure 9. Dependence of $(\hat{P}_{\text{SC/w}})^{\text{comp}}$ upon σ for the (physically unrealistic) case of isotropic lipid-phase diffusion ($D_{\text{trans}} \approx D_{\text{lip}}$). All geometrical parameters (L, t, s, ω, and φ) are adjusted for perfect correspondence with the values assumed by Charalambopoulou et al.[49] Results from the present model (represented as points) agree well with the calculations of these authors[49] (represented as continuous curves). Their model is restricted to the case of isotropic lipid-phase diffusion represented in this figure, whereas ours is not.

address solute permeation into the corneocytes. Their final result (their Eq. 10 or equivalently Eq. 11) applies to the case of unswollen (partially hydrated) skin with 15 layers of corneocytes having a thickness of 0.8 μm. It may be written in the equivalent forms

$$(P_{\text{SC/w}})^{\text{comp}} = D_{\text{lip}} K_{\text{lip/w}}/(3.6\,\text{cm}) \text{ or } (\hat{P}_{\text{SC/w}})^{\text{comp}} = 3.7 \times 10^{-4} \quad (39)$$

translated into the present notation. Their result corresponds to our asymptotic formulas for Model 1 in the limit $\sigma \to \infty$ (see Eqs. A–C in Tab. 3). Neglecting there the quantitatively unimportant term involving L_2', we find

$$(P_{\text{SC/w}})^{\text{comp}} \approx D_{\text{lip}} K_{\text{lip/w}}/(4.6\,\text{cm}) \quad \text{or} \quad (\hat{P}_{\text{SC/w}})^{\text{comp}} \approx 2.9 \times 10^{-4} \quad (40)$$

(Model 1, only lipid lateral diffusion pathway for partially hydrated SC).

Eqs. 39 and 40 would appear in Figure 6 simply as horizontal flat surfaces over the (σ, R) plane, and in Figure 7 as horizontal straight lines over the R axis.

The conclusion to be drawn from this comparison is that, based on a model specifically formulated around an uninterrupted lipid pathway traversable by lateral diffusion, Johnson et al.'s and our estimates of the tortuosity and area fractions of this pathway yield almost identical results. However, such a formulation ignores the rich structure evident in Figures 6 and 7, in which permeation into the corneocytes is rigorously accounted for. Exclusion of such permeation in analyzing SC permeability data is valid only to the extent that the physicochemical properties of any given compound place it well away from the hump in the surface representing $(\hat{P}_{\text{SC/w}})^{\text{comp}}$ (Fig. 6). Our comprehensive treatment of Model 1 provides a basis for this assessment to be made. Model 2 should also be considered, and physical reality probably represents an interpolate between the extremes represented by the two models. Even in cases where asymptotes like Eqs. 39 or 40 might describe $(\hat{P}_{\text{SC/w}})^{\text{comp}}$, solute holdup within the corneocytes can be very substantial; this holdup then just contributes negligibly to the transdermal flux.

For later use we note that the equivalent of Eq. 40 for fully hydrated SC is

$$(P_{\text{SC/w}})^{\text{comp}} \approx D_{\text{lip}} K_{\text{lip/w}}/(5.7\,\text{cm}) \quad \text{or} \quad (\hat{P}_{\text{SC/w}})^{\text{comp}} \approx 7.6 \times 10^{-4} \quad (41)$$

(Model 1, only lipid lateral diffusion pathway for fully hydrated SC).

APPLICATION OF THE MODEL TO ILLUSTRATIVE PERMEANTS

Detailed analysis of an extensive database on SC permeability[54] is presented in the companion study.[55] Nevertheless, it is worthwhile to consider here some illustrative examples in order to demonstrate the application of our model to the interpretation of permeability data for fully hydrated SC. We choose to address the important special case of water permeability, and also three other representative permeants.

Summary of How to Use the Model

For any given permeant, the physicochemical inputs needed to predict $(P_{SC/w})^{comp}$ are the lipid- and corneocyte-phase properties $K_{lip/w}$, D_{lip}, k_{trans}, $K_{cor/w}$, and D_{cor}. They enter the model in the form of the two dimensionless groups σ and R, defined by Eqs. 35 and 38, which determine the dimensionless permeability factor $(\hat{P}_{SC/w})^{comp}$ according to a functional relation presented in readily usable form in Figure 7 (see also the numerical tabulation of $(\hat{P}_{SC/w})^{comp}$ as a function of σ and R given in the Supplementary Material for this article). The dimensional SC permeability coefficient is then given as the product of $(\hat{P}_{SC/w})^{comp}$ and the dimensional factor $D_{lip}K_{lip/w}/h_{SC}$ (Eq. 34). We refer to this predictive procedure as the forward calculation. It may be applied for either partially or fully hydrated skin, and is schematized in Figure 10.

A significant basis in experiment and/or theory exists to generate at least reasonable estimates of the partition and diffusion coefficients, as is discussed in our separate analysis[70] of SC/water partition coefficients and in the companion study to this one.[55] The parameter about which least is known for actual SC lipids is k_{trans}. Our model can actually be used in reverse to deduce values of k_{trans} from measured SC permeabilities. The reverse calculation, also summarized in Figure 10, involves first dividing a measured value of $(P_{SC/w})^{comp}$ by the dimensional factor $D_{lip}K_{lip/w}/h_{SC}$ to produce $(\hat{P}_{SC/w})^{comp}$. (The numerical results for fully hydrated skin will usually be the applicable ones, since the SC is typically fully saturated with water in *in vitro* permeability measurements). Because σ can be estimated, Figure 7 then yields an estimate of R (and thence k_{trans}) as the value of this parameter that reproduces the desired $(\hat{P}_{SC/w})^{comp}$. The examples presented here illustrate this procedure, aimed at gaining quantitative empirical insight into k_{trans}. This application of the model is similar in spirit to Johnson et al.'s[24] deduction of D_{lip} from SC permeability data, within the more limited context of an analysis that presupposes dominance of a lipid-phase lateral diffusion pathway.

Analysis of SC permeability data via the reverse calculation for sufficiently many permeants can produce broad quantitative guidelines and correlations for k_{trans}, for example, as a function of molecular weight.[54,55] With such a correlation in hand, the model acquires predictive power, allowing $(P_{SC/w})^{comp}$ to be estimated for any desired compound via the forward calculation.

Water Permeability

Microscopic phase-specific properties of water are listed in Table 5. As detailed elsewhere,[54,55,70,79] $K_{cor/w}$ results from a view of the corneocyte interior phase as a composite material comprising keratin microfibrils embedded within a connected surrounding aqueous phase. This parameter reflects exclusion from the volume occupied by the keratin (present at a volume fraction of ≈ 0.19 in fully hydrated SC[70]) plus an additional annular volume around each microfibril having thickness equal to the molecular radius (which is negligible for small permeants). D_{cor} reflects aqueous diffusion impeded by a geometrical obstacle factor[79,83,84] imparted by the keratin microfibrils, as well as a water-keratin binding factor.[79] The value listed, equal to 70% of the bulk self-diffusivity at the assumed temperature of 30°C, represents a reasonable estimate by Kasting et al's[79] Method 2 ("modified composite continuum theory"), which is consistent with two spin-echo NMR measurements for mobile protons in guinea pig footpad SC.[85] Here the consideration of water as solute represents the exceptional of case of self-diffusion of tracer water molecules through the aqueous environment. $K_{lip/w}$ comes from the power-law $K_{lip/w} = 0.43(K_{o/w})^{0.81}$, which is the conclusion of a comprehensive new phase-specific analysis[70] of SC/water partition coefficients including the latest available data. Our estimate of D_{lip} is based upon the molecular weight dependence suggested by Johnson et al.'s[24] Figure 2. This figure presents: (i) Johnson et al's[76] video-FRAP measurements of lateral

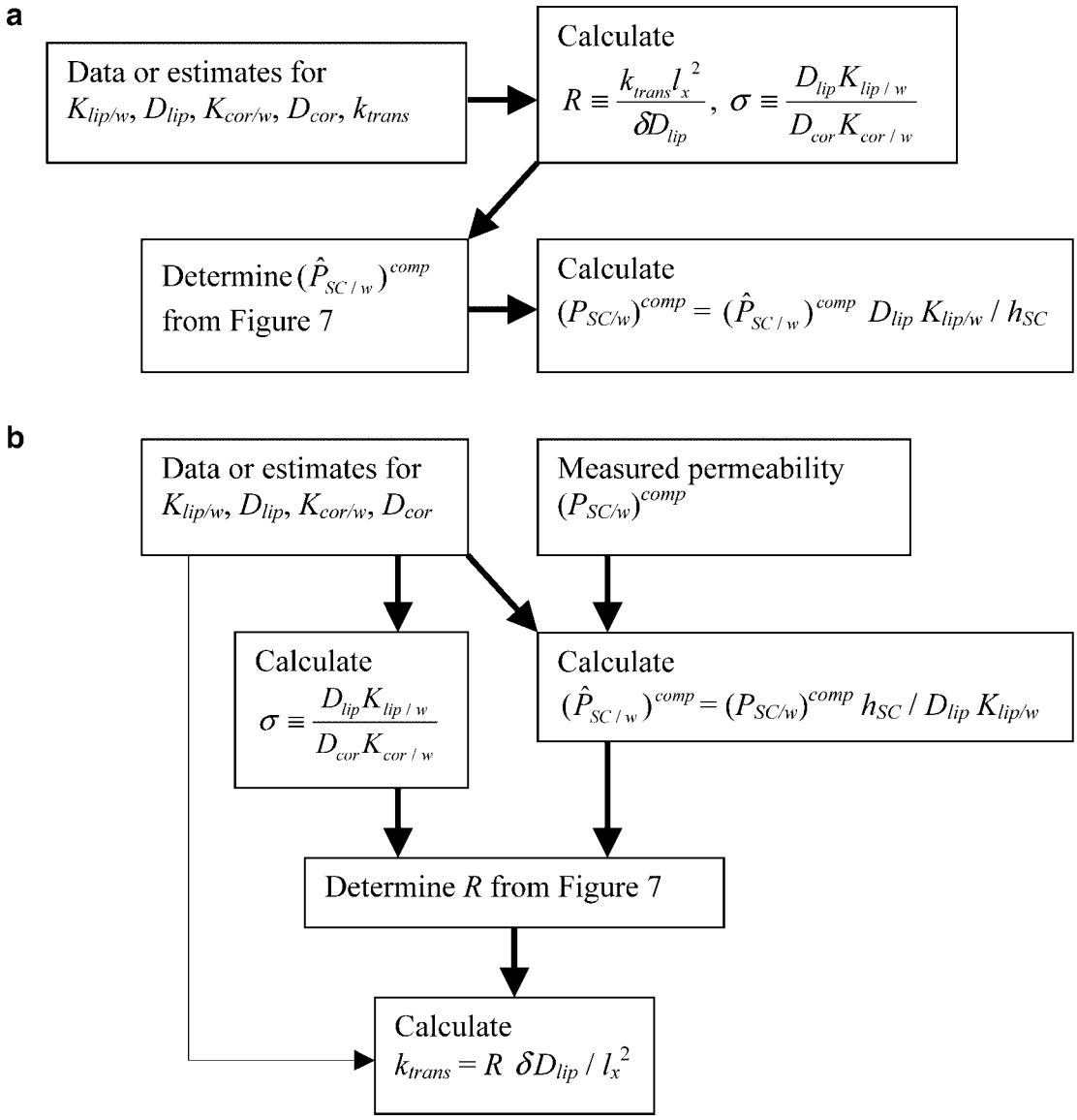

Figure 10. Procedures for (a) the forward calculation and (b) the reverse calculation.

diffusivities of five fluorescent probes within bilayers reconstituted from extracted SC lipids; (ii) a datum for oxygen estimated by applying a tortuosity correction to Hatcher and Plachy's[69] electron paramagnetic resonance measurement of overall effective SC diffusivity; and (iii) Johnson et al.'s[24] derived data on lateral diffusion based on application of their model to an SC permeability database. Of these three sources, only (i) gives direct measurements of D_{lip}. The molecular weight (≈ 220) of even the smallest probe studied greatly exceeds that of water. Also, it is not clear the extent to which the reconstituted SC lipid structure is faithful to *in vivo* structure (although the increased mobility resulting from any possible disruption of structure may mimic the effects of hydration). Although sources (ii) and (iii) fill in the gap in molecular weight, they are potentially colored by a method of analysis that presupposes dominance of a lipid-phase lateral diffusion pathway, as noted by Johnson et al.[24] For all these reasons, the estimate of D_{lip} is uncertain, but the order-of-magnitude value listed in Table 5 accords with available data and experience. An accepted value for SC permeability of water is 1.0×10^{-3} cm/h.[79]

All these inputs yield $\sigma = 0.015$ and $(\hat{P}_{SC/w})^{comp} = 5.1 \times 10^{-3}$. For Model 1, the desired permeability is matched for $R = 680$, corresponding to the dimensional value $k_{trans} = 6.5 \times 10^{-4}$ cm/s.

Table 5. Physicochemical Properties and Outcomes of the Model for Four Illustrative Permeant Compounds

(a) Basic Properties

Permeant	MW	$\log_{10} K_{o/w}$
Water	18	−1.38
Ethanol	46	−0.31
Nicotinamide	122	−0.37
Testosterone	288	3.32

(b) Input Parameters for Model, SC Partition Coefficient Implied by the Model, and Measured SC Permeability

Permeant	$K_{lip/w}$	D_{lip} (cm^2/s)	$K_{cor/w}$	D_{cor} (cm^2/s)	$K_{SC/w}$	$P_{SC/w}$ (cm/h)
Water	0.033	7.2×10^{-6}	0.81	1.9×10^{-5}	0.78	1.0×10^{-3}
Ethanol	0.24	8.5×10^{-7}	0.79	1.2×10^{-5}	0.77	8.0×10^{-4}
Nicotinamide	0.22	9.2×10^{-8}	0.78	7.4×10^{-6}	0.76	4.9×10^{-5}
Testosterone	210	1.3×10^{-8}	0.75	3.5×10^{-6}	8.1	3.8×10^{-3}

Sources for SC permeability are as follows: water from Ref. 79, ethanol and testosterone from Ref. 24, nicotinamide from Ref. 97; permeability of testosterone is the mean of the two values listed in Ref. 24.

(c) Dimensionless Parameters, and Deduced Mass Transfer Coefficient for Transbilayer Hopping

			Model 1		Model 2	
Permeant	σ	$\hat{P}_{SC/w}$	R	k_{trans} (cm/s)	R	k_{trans} (cm/s)
Water	0.015	5.1×10^{-3}	680	6.5×10^{-4}	860	8.2×10^{-4}
Ethanol	0.022	4.7×10^{-3}	620	7.0×10^{-5}	790	8.9×10^{-5}
Nicotinamide	0.0035	3.0×10^{-3}	330	4.1×10^{-6}	480	5.9×10^{-6}
Testosterone	1.0	1.7×10^{-3}	130	2.3×10^{-7}	250	4.3×10^{-7}

The contributions to SC permeability from different elements of the microstructure are quantified by our rigorous treatment of the two-dimensional unit-cell diffusion problem, and are generally not strictly additive. Nevertheless, Eq. 41 (cf. Fig. 7a) leads to the approximate conclusion that just the uninterrupted lipid lateral diffusion pathway could furnish only about 15% ($\approx 8 \times 10^{-4}$) of the observed level of permeability $(\hat{P}_{SC/w})^{comp} = 5.1 \times 10^{-3}$. The difference is made up by transcellular diffusion, which requires transbilayer hopping. The hopping process is rate limiting (the corneocytes being effectively transparent to water), and the calculated k_{trans} represents the value needed for the transcellular pathway to provide the required additional flux. The full level of permeability could also be explained by just the lipid lateral diffusion pathway using a more generous estimate for D_{lip} (increased by a factor of about 7). Indeed, Johnson et al.[24] effectively explain the observed water permeability of the SC in this way. However, even our original estimate $D_{lip} = 7.2 \times 10^{-6}$ cm^2/s seems overly generous in view of the fact that the diffusivity of water in, for example, bulk liquid butanol is only 0.56×10^{-5} cm^2/s at 25°C (Ref. 86, p 11.31; a temperature correction yields 0.64×10^{-5} cm^2/s at 30°C).

According to Model 2, the desired permeability is matched for $R = 860$, corresponding to the dimensional value $k_{trans} = 8.2 \times 10^{-4}$ cm/s. Both lipid lateral diffusion and transcellullar pathways are interrupted by transbilayer hopping, which is rate limiting for both pathways. Because σ (0.015) is so much smaller than the critical value $\sigma_{cutoff} \approx 1200$ (for fully hydrated SC), by far most of the water passes through the corneocytes. Because the corneocytes are transparent (highly permeable relative to the transbilayer interfaces), the SC barrier is effectively provided by the $15 \times 7 = 105$ such interfaces. The position of water in the dimensionless parameter space as described by this model is marked in Figure 6c.

Although no direct data on SC lipids exist for comparison, it is worth noting the estimates of k_{trans} deriving from both models are somewhat smaller than, but within an order of magnitude of, a measured water permeability of egg

phosphatidylcholine bilayers (3.4×10^{-3} cm/s)[87] cited by Mitragotri et al.[73]

Other Illustrative Compounds

The further compounds considered here are ethanol, nicotinamide, and testosterone, for which physicochemical properties are listed in Table 5. Their molecular weights and octanol/water partition coefficients[88] give an indication of molecular size and lipophilicity. Ethanol and nicotinamide are very similarly hydrophilic ($\log_{10} K_{o/w} = -0.31$ and -0.37, respectively), but differ significantly in molecular size, nicotinamide having almost triple the molecular weight of ethanol. Due to its smaller size, the diffusivity of ethanol in both lipid and corneocyte phases is larger than that of nicotinamide. Judging by the small value of σ, corneocyte permeability plays a major role for nicotinamide. The value of σ for ethanol is larger not because of any dramatic corneocyte-phase property differences, but rather because D_{lip} is a strong function of molecular weight, and therefore much larger for ethanol than for nicotinamide. Nevertheless, the corneocyte phase is still very accessible to ethanol. Testosterone is very lipophilic ($\log_{10} K_{o/w} = 3.32$), greatly enhancing its solubility in the intercellular lipid phase. It is also the largest of the three molecules, and therefore has the lowest diffusivities in both lipid and corneocyte phases. Despite its lipophilicity, σ is still only 1.0 for this compound. Values of $K_{cor/w}$ and D_{cor} for the larger permeants (especially testosterone) incorporate additional volumetric exclusion, as well as significant hydrodynamic hindrance effects in the case of D_{cor}, associated with finite molecular size, the latter estimated on the basis of Phillips et al's rigorous analysis of hindered diffusion in media with fibrous obstacles.[89] It is worth noting that, for the additional three compounds considered, the estimated values of $K_{cor/w}$ and D_{cor} in Table 5 refer to free (mobile) solute. Binding to constituents of the corneocyte phase increases holdup in this phase, but does not contribute to flux. As noted earlier, only the product $K_{cor/w}D_{cor}$ enters the calculation of permeability, not the individual factors separately. This product, representing corneocyte permeability, is effectively independent of binding at low solute concentrations, for which binding can be described by a partition coefficient (or linear isotherm).

The same computational procedure as for water yields the results listed in Table 5 and the positions of the compounds in the dimensionless parameter space are also marked in Figure 6c. Transbilayer hopping steps exist as interruptions of both transcellular and lipid paths in Model 2, but only the trancellular path in Model 1. This is the reason why Model 2 leads to larger estimates of k_{trans} than Model 1, needed to describe the observed levels of permeability. Figure 11 shows that the derived estimates of k_{trans} decrease monotonically with increasing solute molecular weight, as expected since the difficulty of permeating between adjacent chains in the transitional tight hydrocarbon zones should increase with increasing molecular size. Even for testosterone, since σ is much smaller than $\sigma_{cutoff} \approx 500$ (for fully hydrated SC), the bulk of the solute flux occurs transcellularly, and the corneocytes are effectively transparent. The lipid phase still controls SC permeability, albeit via the barrier associated with transbilayer hopping as opposed to lateral diffusion. This logical conclusion for testosterone controverts often-repeated doctrine regarding intercellular penetration pathways of lipophilic compounds; it could only be precluded by (1) an additional diffusion barrier provided by the cornified cell envelope or (2) a substantial salting out effect of the intracorneocyte electrolyte. The transcellular pathway was first recognized and developed theoretically in an early analysis by Yotsuyanagi and Higuchi,[51] which far predates recent models[24,30,32] emphasizing the lipid lateral diffusion pathway.

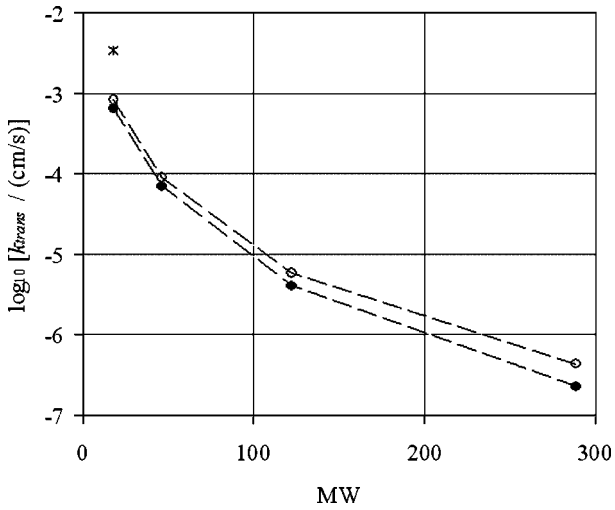

Figure 11. Dependence of derived estimates of k_{trans} upon molecular weight for Model 1 (filled circles (●)) and Model 2 (open circles (○)). A measured water permeability of egg phosphatidylcholine bilayers (3.4×10^{-3} cm/s)[87] cited by Mitragotri et al.,[73] is shown for comparison (asterisk (*)).

DISCUSSION

The preceding text has developed a detailed model of SC permeability having a firm basis in a realistic representation of the multiphase SC microstructure, subjected to rigorous numerical and asymptotic analysis. The final outcome comprises quantitative numerical data on the functional dependence of SC permeability upon the two key dimensionless groups, namely R (containing k_{trans}) and σ (expressing the ratio of lipid- to corneocyte-phase permeabilities). These results are uncolored by any analytical approximations in solving the model equations, or any *a priori* assumptions regarding occupancy of, or transport within, the lipid and corneocyte phases. Aside from specific numerical values, the analysis gives a comprehensive view of the physicochemical parameter space (Fig. 6).

It is worth emphasizing that the present model addresses the intrinsic permeability of an intact SC. As such, it provides a basis for understanding quantitatively how skin appendages increase SC permeability via shunt pathways. Indeed, only if $(P_{\mathrm{SC/w}})^{\mathrm{comp}}$ is known can it be subtracted from the total observed permeability $P_{\mathrm{SC/w}}$ to estimate contributions from appendageal pathways (cf. Eq. 2).

Real SC microstructure comprises a three-dimensional arrangement of roughly polygonal corneocytes, and the relation between two and three-dimensional representations of it is clearly an important subject for continuing study.[54] Nevertheless, two-dimensional models can offer a very useful, quantitative basis for understanding and predicting SC permeability. Indeed, flux via the lipid pathway is largely determined by its area fraction and tortuosity;[24,26,29,31,44,46,52] thus, a two dimensional model will offer a realistic representation of this component if it reproduces these structural features. Also, the transcellular pathway involves largely one-dimensional traversal of alternating corneocyte and lipid lamellae,[51,79] for which the shapes or arrangement of the corneocytes in the plane of the skin is unimportant.

Application of our model to a large database on SC permeability[54] is the subject of a companion study,[55] which develops general procedures for estimating the requisite physicochemical inputs ($K_{\mathrm{lip/w}}$, D_{lip}, $K_{\mathrm{cor/w}}$, D_{cor}) in terms of permeant structure and properties. Analysis of SC permeability data via the reverse calculation (Fig. 10b) for sufficiently many permeants can produce a broad quantitative understanding of k_{trans}, and correlations for k_{trans} as a function of molecular properties. Figure 11 is suggestive of such a correlation. With the accumulation of this type of information, the model acquires predictive power, allowing $(P_{\mathrm{SC/w}})^{\mathrm{comp}}$ to be estimated for any desired compound via the forward calculation.

Lipid-Phase Topology

Two extremes of lipid-phase topology have been considered. Model 1 is specifically formulated to furnish an uninterrupted lipid pathway traversable purely by lateral diffusion. In Model 2 each corneocyte is completely surrounded by intact lipid bilayers, and progress from one layer of corneocytes to the next requires transbilayer hopping. The two lipid-phase topologies lead to essentially identical permeability behavior for large values of k_{trans} (or large R), but dramatically different behavior for small values of k_{trans} (or small R).

Models 1 and 2 can be used to analyze measured SC permeabilities with a view toward elucidating microscopic phase-specific transport parameters like k_{trans}. For either one, the analysis accounts rigorously for the contributions of both lipid and corneocyte phases, and yields valuable conclusions. For instance, by a reasonable parametrization of both models it is found that most permeating water must diffuse transcellularly. This statement agrees with a similar conclusion about water permeability reached by Kasting et al. (2003).[79] Physical reality is probably best regarded as a composite of the two extremes considered. Model 2 may be the more realistic, because it is a valid question why such a key physiological barrier as the SC would have a structure optimized for high permeability by an uninterrupted path. Thus, even in cases where the lipid pathway might dominate solute flux, transport could occur by a combination of lateral diffusion and transbilayer hopping, the latter process furnishing the barrier function. Resolution of an effective average lipid-phase topology is clearly an important question for further study drawing on structural characterizations.

Corneocyte-Phase Holdup

Our analysis allows explicitly for possible occupancy of both the intercellular lipid and corneocytes by solute. We make no *a priori* assumptions about the respective roles played by these two phases. Rather, their relative contributions to

$(P_{SC/w})^{comp}$ emerge naturally as an outcome of the analysis.

Due to the large volume fraction of corneocytes, it does not require a high partition ratio into the corneocyte phase to have significant occupancy of this phase, as reflected in $K_{SC/w}$ (see Eq. 5). This fact combined with limitations on dynamic range may help to reconcile the present conclusion regarding solute entry into corneocytes with microscopy studies in which they appear to be largely excluded.[27,90–94] The latter reports are furthermore balanced by more recent studies employing two-photon fluorescence measurements in which partial entry of both hydrophilic and hydrophobic substances[95] as well as a pH-sensitive dye[96] into corneocytes was documented, and by Anderson et al.'s work on SC structure-permeability-partition relationships.[35,37,43] Additional discussion of this subject has been offered elsewhere.[97] There should be no reluctance to consider corneocyte-phase holdup, even for lipophilic compounds, because corneocyte-phase holdup is not synonymous with corneocyte-phase flux.

Effective Diffusivity and Lag Time

The quantity of primary interest, the steady state permeability coefficient $(P_{SC/w})^{comp}$, is determined by a flux calculation (see Eqs. 32–34). Its numerical determination, as well as use as the constant of proportionality between solute concentration difference and flux across the SC (Eq. 1), does not require any explicit decomposition into $K_{SC/w}$ and D_{SC} factors. Nevertheless, our model does furnish a self-consistent method for making this decomposition. Indeed, after determining $(P_{SC/w})^{comp}$ by the forward calculation (see Fig. 10a), the effective diffusivity can be obtained by rearranging Eq. 3 as

$$D_{SC} = (P_{SC/w})^{comp} h_{SC}/K_{SC/w}. \qquad (42)$$

Here $h_{SC} = N_{layer}\, m_y = 15\ (t+s) = 13.4$ or 43.4 μm for partially or fully hydrated skin, respectively, and $K_{SC/w}$ is given by Eq. 5.

Although D_{SC} is derived from a steady state analysis, it would in principle serve to describe transient penetration. This conclusion follows from the fact that the general prescription for calculating effective diffusivities based on the long-time asymptotic behavior of the transient solute spreading process[57,58] can be shown to be mathematically equivalent to the steady state prescription employed here[56] (cf. Appendix of Ref. 98). The caveat to this statement is that penetration occurs macroscopically as a diffusive process characterized by D_{SC} only at times well over the diffusive relaxation time for equilibration of solute within one unit cell (i.e., one layer of corneocytes). Furthermore, this statement applies to situations where there is no binding or else effectively instantaneous binding; if any corneocyte-phase binding processes equilibrate slowly, then their transients would also come into play. These caveats cloud the application of the macroscopic average D_{SC} to quantify transient penetration (as distinct from steady flux) through the SC, especially at short times following drug application or chemical exposure. The only unambiguous way of treating transient aspects of solute penetration, such as the lag time needed for a state of steady flux through the SC to be established,[2,32,36,67,99] is to retreat from the macroscopic (effective transport) approach, and rather calculate explicitly the transient evolution of the microscopic solute concentration field within a sequence of unit cells, as was done by Heisig et al.[48] for their brick-and-mortar model.

The reason for mentioning transient penetration here is to make an important qualitative point concerning lag times for dermal penetration vis-à-vis corneocyte-phase holdup. Analyses focusing on the lipid pathway generally do not address explicitly the question of possible holdup of solute in the corneocytes. In general (even in a circumstance where the lipid phase might dominate solute flux for a very lipophilic solute according to Model 1), it is a mistake to ignore this holdup. To do so would be to replace Eq. 5 with the incomplete statement

$$K_{SC/w} = \phi_{lip} K_{lip/w} \ \begin{pmatrix}\text{ignoring corneocyte-}\\ \text{phase solute holdup}\end{pmatrix}. \qquad (5a)$$

This incomplete variant of Eq. 5 yields much smaller values of $K_{SC/w}$, because of the smallness of ϕ_{lip}, except for very lipophilic permeants (for which the lipid-phase term dominates since $K_{lip/w}$ is so large). In order to maintain the same product $K_{SC/w}D_{SC}$, the implied value of D_{SC} must be larger, which decreases the predicted lag time. The problem that consideration of just the lipid phase yields overly short predicted lag times is well recognized.[24,79] Explicit recognition of solute holdup in the corneocytes leads to a decomposition of the steady state permeability into $K_{SC/w}$ and D_{SC} factors with smaller values of D_{SC}, which tends to bring calculated lag times into better agreement with observations (calculations not shown).

NOMENCLATURE

Definitions are given for the most important symbols used in the text.

Roman Symbols

C_{cor}	superficial concentration (total moles of solute per total volume) within the corneocyte phase
$C_{lip,i}$	cross-sectional average solute concentration within lipid bilayer i considered as a one-dimensional distribution
D_{cor}	corneocyte-phase diffusion coefficient based on superficial concentration within this phase
D_{lip}	diffusion coefficient for lateral diffusion within SC lipid
D_{SC}	effective diffusion coefficient of the SC considered macroscopically as a composite continuum
h_{SC}	thickness of the SC
$K_{cor/w}$, $K_{lip/w}$	partition coefficients for corneocyte and lipid phases, respectively, relative to an aqueous solution (w) at a prescribed pH
$K_{o/w}$	octanol/water partition coefficient
$K_{SC/w}$	average SC/water partition coefficient for the SC considered macroscopically as a composite continuum
k_{trans}	mass transfer coefficient for transbilayer hopping
$\mathbf{l}$, $\mathbf{m}$	lattice vectors defining the assumed periodicity of the model SC microstructure ($\mathbf{l} = l_x\mathbf{i} + 0\mathbf{j}$, $\mathbf{m} = m_x\mathbf{i} + m_y\mathbf{j}$)
N_{layer}	number of cell layers in the SC
$(P_{SC/w})^{comp}$	permeability coefficient of the SC, representing the constant of proportionality between permeant flux J (mol/cm$^2 \cdot$ s) through a defect-free, appendage-free SC sample, and the driving difference in permeant concentrations between two aqueous solutions separated by the sample
R	dimensionless parameter representing a ratio of transbilayer to lateral molecular flows within a lipid bilayer ($R = k_{trans}\, l_x^2/(\delta\, D_{lip})$)
s	thickness of intercellular lipid phase
x, y	cartesian coordinates
z	linear coordinate running along a lipid bilayer

Greek Symbols

δ	thickness of a lipid bilayer
φ	angle of inclination of slanted lipid bilayer segment relative to the horizontal
σ	dimensionless paramerer representing the ratio of (lateral) permeability in the lipid phase to that in the corneocyte phase ($\sigma = D_{lip}K_{lip/w}/(D_{cor}K_{cor/w})$)

Subscripts and Affixes

i	index identifying a specific lipid bilayer
j	index identifying an envelope-lipid monolayer
^	distinguishes dimensionless variables
−	distinguishes macroscopic average quantities

ACKNOWLEDGMENTS

We gratefully acknowledge financial support of this work from the Procter & Gamble Company's International Program for Animal Alternatives, NSF GOALI grant BES-9818160, and NIOSH grant R01 OH007529.

REFERENCES

1. Blank IH, Scheuplein RJ. 1969. Transport into and within the skin. Br J Derm 81(Suppl. 4):4–10.
2. Scheuplein RJ, Blank IH. 1971. Permeability of the skin. Physiol Rev 51:702–747.
3. Wester RC, Maibach HI. 1983. Cutaneous pharmacokinetics: 10 steps to percutaneous absorption. Drug Metabolism Rev 14:169–205.
4. Ritschel WA, Hussain AS. 1988. The principles of permeation of substances across the skin. Meth Find Exptl Clin Pharmacol 10:39–56.
5. Wester RC, Maibach HI. 1992. Percutaneous absorption of drugs. Clin Pharmacokinet 23:253–266.
6. Siddiqui O. 1989. Physicochemical, physiological, and mathematical considerations in optimizing percutaneous absorption of drugs. Crit Rev Ther Drug Carrier Syst 6:1–38.

7. Wiechers JW. 1989. The barrier function of the skin in relation to percutaneous absorption of drugs. Pharm Weekbl Sci 11:185–198.
8. Robinson PJ. 1998. Prediction: simple risk models and overview of dermal risk assessment, Chapter 8. In: Roberts MS, Walters KA, editors. Dermal absorption and toxicity assessment. New York: Marcel Dekker, pp 203–229.
9. Gerberick GF, Robinson MK, Felter SP, White IR, Basketter DA. 2001. Understanding fragrance allergy using an exposure-based risk assessment approach. Contact Derm 45:333–340.
10. Montagna W, Parakkal PF. 1974. The structure and function of skin, 3rd edn. New York: Academic Press.
11. Roberts MS, Walters KA. 1998. The relationship between structure and barrier function of skin, Chapter 1. In: Roberts MS, Walters KA, editors. Dermal absorption and toxicity assessment. New York: Marcel Dekker, pp 1–42.
12. Feldman RJ, Maibach HI. 1970. Absorption of some organic compounds through the skin in man. J Invest Dermatol 54:399–404.
13. Zhen Y-X, Suetake T, Tagami H. 1999. Number of cell layers of the stratum corneum in normal skin - relationship to the anatomical location on the body, age, sex and physical parameters. Arch Dermatol Res 291:555–559.
14. Hou SYE, Rehfeld SJ, Plachy WZ. 1991. X-ray diffraction and electron paramagnetic resonance spectroscopy of mammalian stratum corneum lipid domains. In: Elias PM, editor. Adv lipid res, vol. 24: skin lipids. New York: Academic Press, pp 141–171.
15. Ribaud C, Garson J-C, Doucet J, Lévêque J-L. 1994. Organization of stratum corneum lipids in relation to permeability: influence of sodium lauryl sulfate and preheating. Pharm Res 11:1414–1418.
16. Brody I. 1960. The ultrastructure of the tonofibrils in the keratinization process of normal human epidermis. J Ultrastruct Res 4:264–297.
17. Potts RO, Guy RH. 1992. Predicting skin permeability. Pharm Res 9:663–669.
18. Guy RH, Potts RO. 1992. Structure-permeability relationships in percutaneous penetration. J Pharm Sci 81:603–604.
19. Kasting GB, Smith RL, Anderson BD. 1992. Prodrugs for dermal delivery: solubility, molecular size, and functional group effects, Chapter 3. In: Sloan KB, editor. Prodrugs: topical and Ocular Drug Delivery. New York: Marcel Dekker, pp 117–161.
20. Hostýnek JJ, Reifenrath WG, Melendres JL, Magee PS. 1995. Correlation of in vivo and in vitro percutaneous absorption with a mathematical model. In: Surber C, Elsner P, Bircher AJ, editors. Curr prob dermatol, vol. 22: exogenous dermatology. Basel: Karger, pp 139–145.
21. Potts RO, Guy RH. 1995. A predictive algorithm for skin permeability: the effects of molecular size and hydrogen bond activity. Pharm Res 12:1628–1633.
22. Wilschut A, ten Berge WF, Robinson PJ, McKone TE. 1995. Estimating skin permeation. The validation of five mathematical skin permeation models. Chemosphere 30:1275–1296.
23. Flynn GL. 1990. Physicochemical determinants of skin absorption. In: Gerrity TR, Henry CJ, editors. Principles of route-to-route extrapolation for risk assessment. New York: Elsevier, pp 93–127.
24. Johnson ME, Blankschtein D, Langer R. 1997. Evaluation of solute permeation through the stratum corneum: lateral bilayer diffusion as the primary transport mechanism. J Pharm Sci 86: 1162–1172.
25. Elias PM. 1981. Lipids and the epidermal permeability barrier. Arch Dermatol Res 270:95–117.
26. Albery WJ, Hadgraft J. 1979. Percutaneous absorption: in vivo experiments. J Pharm Pharmacol 31: 140–147.
27. Boddé HE, van den Brink I, Koerten HK, de Haan FHN. 1991. Visualization of in vitro percutaneous penetration of mercuric chloride; transport through intercellular space versus cellular uptake through desmosomes. J Control Release 15:227–236.
28. Elias PM, Friend DS. 1979. The permeability barrier in mammalian epidermis. J Cell Biol 65: 180–191.
29. Potts RO, Francoeur ML. 1991. The influence of stratum corneum morphology on water permeability. J Invest Dermatol 96:495–499.
30. Mitragotri S. 2002. A theoretical analysis of permeation of small hydrophobic solutes across the stratum corneum based on scaled particle theory. J Pharm Sci 91:744–752.
31. Lange-Lieckfeldt R, Lee G. 1992. Use of a model lipid matrix to demonstrate the dependence of the stratum corneum's barrier properties on its internal geometry. J Control Release 20:183–194.
32. Frasch HF, Barbero AM. 2003. Steady-state flux and lag time in the stratum corneum lipid pathway: results from finite element models. J Pharm Sci 92: 2196–2207.
33. Peck KD, Ghanem A-H, Higuchi WI. 1994. Hindered diffusion of polar molecules through and effective pore radii estimates of intact and ethanol treated human epidermal membrane. Pharm Res 11:1306–1314.
34. Ackermann C, Flynn GL. 1987. Ether–water partitioning and permeability through nude mouse skin in vitro. I. Urea, thiourea, glycerol and glucose. Int J Pharm 36:61–66.
35. Anderson BD, Raykar PV. 1989. Solute structure–permeability relationships in human stratum corneum. J Invest Dermatol 93:280–286.
36. Scheuplein RJ. 1967. Mechanism of percutaneous absorption. II. Transient diffusion and the relative importance of various routes of skin penetration. J Invest Dermatol 48:79–88.
37. Anderson BD, Higuchi WI, Raykar PV. 1988. Heterogeneity effects on permeability—partition

coefficient relationships in human stratum corneum. Pharm Res 5:566–573.
38. Kim Y-H, Ghanem A-H, Mahmoud H, Higuchi WI. 1992. Short chain alkanols as transport enhancers for lipophilic and polar/ionic permeants in hairless mouse skin: mechanism(s) of action. Int J Pharm 80:17–31.
39. Hatanaka T, Manabe E, Sugibayashi K, Morimoto Y. 1994. An application of the hydrodynamic pore theory to percutaneous absorption of drugs. Pharm Res 11:654–658.
40. Yamashita F, Bando H, Koyama Y, Kitagawa S, Takakura Y, Hashida M. 1994. In vivo and in vitro analysis of skin penetration enhancement based on a two-layer diffusion model with polar and nonpolar routes in the stratum corneum. Pharm Res 11:185–191.
41. Yoneto K, Ghanem A-H, Higuchi WI, Peck KD, Li SK. 1995. Mechanistic studies of the 1-alkyl-2-pyrrolidones as skin permeation enhancers. J Pharm Sci 84:312–317.
42. Lee AJ, King JR, Barrett DA. 1997. Percutaneous absorption: a multiple pathway model. J Control Release 45:141–151.
43. Raykar PV, Fung M-C, Anderson BD. 1988. The role of protein and lipid domains in the uptake of solutes by human stratum corneum. Pharm Res 5:140–150.
44. Michaels AS, Chandrasekaran SK, Shaw JE. 1975. Drug permeation through human skin: theory and in vitro experimental measurement. AIChE J 21: 985–996.
45. Albery WJ, Hadgraft J. 1979. Percutaneous absorption: theoretical description. J Pharm Pharmacol 31:129–139.
46. Tojo K. 1987. Random brick model for drug transport across stratum corneum. J Pharm Sci 76:889–891.
47. Edwards DA, Langer R. 1994. A linear theory of transdermal transport phenomena. J Pharm Sci 83: 1315–1334.
48. Heisig M, Lieckfeldt R, Wittum G, Mazurkevich G, Lee G. 1996. Non steady-state descriptions of drug permeation through stratum corneum. I. The biphasic brick-and-mortar model. Pharm Res 13:421–426.
49. Charalambopoulou GCh, Karamertzanis P, Kikkinides ES, Stubos AK, Kanellopoulos NK, Papaioannou ATh. 2000. A study on structural and diffusion properties of porcine stratum corneum based on very small angle neutron scattering data. Pharm Res 17:1085–1091.
50. Frasch HF. 2002. A random walk model of skin permeation. Risk Analysis 22:265–276.
51. Yotsuyanagi T, Higuchi WI. 1972. A two phase series model for the transport of steroids across the fully hydrated stratum corneum. J Pharm Pharmac 24:934–941.
52. Lieckfeldt R, Lee G. 1995. Measuring the diffusional pathlength and area within membranes of excised human stratum corneum. J Pharm Pharmacol 47:26–29.
53. Talreja PS, Kleene NK, Pickens WL, Wang T-F, Kasting GB. 2001. Visualization of the lipid barrier and measurement of lipid pathlength in human stratum corneum. AAPS Pharm Sci 3: Article 13.
54. Wang T-F. 2003. Microscopic models for the structure and permeability of the stratum corneum barrier layer of skin. Ph.D. thesis, University at Buffalo, State University of New York.
55. Wang T-F, Kasting GB, Nitsche JM. A multiphase microscopic model for stratum corneum permeability. II. Estimation of physicochemical parameters, and application to a large permeability database. J Pharm Sci (submitted).
56. Jackson JL, Coriell SR. 1963. Effective diffusion constant in a polyelectrolyte solution. J Chem Phys 38:959–968.
57. Brenner H, Edwards DA. 1993. Macrotransport processes. Boston: Butterworth-Heinemann.
58. Brenner H, Adler PM. 1982. Dispersion resulting from flow through spatially periodic porous media. II. Surface and intraparticle transport. Phil Trans R Soc London A 307:149–200.
59. Warner RR, Myers MC, Taylor DA. 1988. Electron probe analysis of human skin: determination of the water concentration profile. J Invest Dermatol 90: 218–224.
60. Caspers PJ, Lucassen GW, Bruining HA, Puppels GJ. 2000. Automated depth-scanning confocal Raman microspectrometer for rapid in vivo determination of water concentration profiles in human skin. J Raman Spectrosc 31:813–818.
61. Kasting GB, Barai ND. 2003. Equilibrium water sorption in human stratum corneum. J Pharm Sci 92:1624–1631.
62. Bouwstra JA, de Graaff A, Gooris GS, Nijsse J, Wiechers JW, van Aelst AC. 2003. Water distribution and related morphology in human stratum corneum at different hydration levels. J Invest Dermatol 120:750–758.
63. Warner RR, Stone KJ, Boissy YL. 2003. Hydration disrupts human stratum corneum ultrastructure. J Invest Dermatol 120:275–284.
64. Anissimov YG, Roberts MS. 2004. Diffusion modeling of percutaneous absorption kinetics: 3. Variable diffusion and partition coefficients, consequences for stratum corneum depth profiles and desorption kinetics. J Pharm Sci 93:470–487.
65. Mueller B, Anissimov YG, Roberts MS. 2003. Unexpected clobetasol propionate profile in human stratum corneum after topical application in vitro. Pharm Res 20:1835–1837.
66. Cleek RL, Bunge AL. 1993. A new method for estimating dermal absorption from chemical exposure. 1. General approach. Pharm Res 10:497–506.
67. Bunge AL, Cleek RL. 1995. A new method for estimating dermal absorption from chemical exposure: 2.

Effect of molecular weight and octanol-water partitioning. Pharm Res 12:88–95.
68. Bouwstra JA, Gooris GS, van der Spek JA, Bras W. 1991. Structural investigations of human stratum corneum by small-angle X-ray scattering. J Invest Dermatol 97:1005–1012.
69. Hatcher ME, Plachy WZ. 1993. Dioxygen diffusion in the stratum corneum: an EPR spin label study. Biochim Biophys Acta 1149:73–78.
70. Nitsche JM, Wang TF, Kasting GB. 2006. A two-phase analysis of solute partitioning into the stratum corneum. J Pharm Sci 95:649–666.
71. Jin B, Hopfinger AJ. 1996. Characterization of lipid membrane dynamics by simulation: 3. Probing molecular transport across the phospholipid bilayer. Pharm Res 13:1786–1794.
72. Marrink S-J, Berendsen HJC. 1994. Simulation of water transport through a lipid membrane. J Phys Chem 98:4155–4168.
73. Mitragotri S, Johnson ME, Blankschtein D, Langer R. 1999. An analysis of the size selectivity of solute partitioning, diffusion, and permeation across lipid bilayers. Biophys J 77:1268–1283.
74. Haines TH, Liebovitch LS. 1995. A molecular mechanism for the transport of water across phospholipid bilayers, Chapter 6. In: Disalvo EA, Simon SA, editors. Permeability and stability of lipid bilayers. Boca Raton, FL: CRC Press, pp 123–136.
75. Träuble H. 1971. The movement of molecules across lipid membranes: a molecular theory. J Membrane Biol 4:193–208.
76. Johnson ME, Berk DA, Blankschtein D, Golan DE, Jain RK, Langer RS. 1996. Lateral diffusion of small compounds in human stratum corneum and model lipid bilayer systems. Biophys J 71:2656–2668.
77. Saffman PG, Delbrück M. 1975. Brownian motion in biological membranes. Proc Natl Acad Sci USA 72:3111–3113.
78. Nemes Z, Steinert PM. 1999. Bricks and mortar of the epidermal barrier. Exp Molecular Med 31:5–19.
79. Kasting GB, Barai ND, Wang T-F, Nitsche JM. 2003. Mobility of water in human stratum corneum. J Pharm Sci 92:2326–2340.
80. Swartzendruber DC, Wertz PW, Madison KC, Downing DT. 1987. Evidence that the corneocyte has a chemically bound lipid envelope. J Invest Dermatol 88:709–713.
81. Abdulmajed K, Heard CM, McGuigan C, Pugh WJ. 2004. Topical delivery of retinyl ascorbate co-drug. 2. Comparative skin tissue and keratin binding studies. Skin Pharmacol Physiol 17:274–282.
82. Guo X, Imhof RE, de Rigal J. 2001. Spectroscopic study of water-keratin interactions in stratum corneum. Analytical Sciences 17:s342–s345.
83. Tomadakis MM, Sotirchos SV. 1993. Transport properties of random arrays of freely overlapping cylinders with various orientation distributions. J Chem Phys 98:616–626.
84. Mottram JT, Taylor R. 1987. Thermal conductivity of fibre-phenolic resin composites. Part II: numerical evaluation. Compos Sci Tech 29:211–232.
85. Packer KJ, Sellwood TC. 1978. Proton magnetic resonance studies of hydrated stratum corneum. Part 2.—Self-diffusion. J Chem Soc Faraday Trans II 74:1592–1606.
86. Poling BE, Prausnitz JM, O'Connell JP. 2001. The properties of gases and liquids, 5th edn. New York: McGraw-Hill.
87. de Gier J. 1993. Osmotic behaviour and permeability properties of liposomes. Chem Phys Lip 64:187–196.
88. MEDCHEM database and CLOGP Program Vers 2.0.0. 1999. Claremont, CA: BioByte, Inc.
89. Phillips RJ, Deen WM, Brady JF. 1990. Hindered transport in fibrous membranes and gels: effect of solute size and fiber configuration. J Colloid Interface Sci 139:363–373.
90. Nemanic MK, Elias PM. 1980. In situ precipitation: a novel cytochemical technique for visualization of permeability pathways in mammalian stratum corneum. J Histochem Cytochem 28:573–578.
91. Monteiro-Riviere NA, Inman AO, Riviere JE. 1994. Identification of the pathway of iontophoretic drug delivery: light and ultrastructural studies using mercuric chloride in pigs. Pharm Res 11:251–256.
92. Menon GK, Bommannan DB, Elias PM. 1994. High-frequency sonophoresis: permeation pathways and structural basis for enhanced permeability. Skin Pharmacol 7:130–139.
93. Simonetti O, Hoogstraate AJ, Bialik W, Kempenaar JA, Schrijvers AHGJ, Boddé HE, Ponec M. 1995. Visualization of diffusion pathways across the stratum corneum of native and in-vitro-reconstructed epidermis by confocal laser scanning microscopy. Arch Dermatol Res 287:465–473.
94. Menon GK, Elias PM. 1997. Morphologic basis for a pore-pathway in mammalian stratum corneum. Skin Pharmacol 10:235–246.
95. Yu B, Kim KH, So PTC, Blankschtein D, Langer R. 2003. Visualization of oleic acid-induced transdermal diffusion pathways using two-photon fluorescence microscopy. J Invest Dermatol 120:448–455.
96. Hanson KM, Behne MJ, Barry NP, Mauro TM, Gratton E, Clegg RM. 2002. Two-photon fluorescence lifetime imaging of the skin stratum corneum pH gradient. Biophys J 83:1682–1690.
97. Kasting GB, Miller MM, Talreja PS. 2005. Evaluation of stratum corneum heterogeneity. In: Bronaugh RL, Maibach HI, editors. Percutaneous absorption. New York: Taylor and Francis, pp 193–212.
98. Nitsche JM. 1991. Hydrodynamic coupling and non-equilibrium distribution in pore diffusion of nonspherical fine particles. Particulate Sci Technol 9:135–148.
99. Perry D, Ward WJ, Cussler EL. 1989. Unsteady diffusion in barrier membranes. J Membrane Sci 44:305–311.